






## Article

# On the Control and Validation of the PARA-SILSROB Surgical Parallel Robot

Doina Pisla <sup>1</sup>, Calin Popa <sup>1,2</sup>, Alexandru Pusca <sup>1</sup>, Andra Ciocan <sup>1,2</sup>, Bogdan Gherman <sup>1,\*</sup>, Emil Mois <sup>1,2</sup>, Andrei-Daniel Cailean <sup>1</sup>, Calin Vaida <sup>1</sup>, Corina Radu <sup>1,3</sup>, Damien Chablat <sup>1,4</sup> and Nadim Al Hajjar <sup>1,2</sup>

- <sup>1</sup> CESTER Department, Technical University of Cluj-Napoca, 400114 Cluj-Napoca, Romania; doina.pisla@mep.utcluj.ro (D.P.); calin.popa@umfcluj.ro (C.P.); alexandru.pusca@mep.utcluj.ro (A.P.); andra.ciocan@umfcluj.ro (A.C.); emil.mois@umfcluj.ro (E.M.); andrei.cailean@mep.utcluj.ro (A.-D.C.); calin.vaida@mep.utcluj.ro (C.V.); corina.radu@umfcluj.ro (C.R.); damien.chablat@cnrs.fr (D.C.); na.hajjar@umfcluj.ro (N.A.H.)
- <sup>2</sup> Department of Surgery, “Iuliu Hatieganu” University of Medicine and Pharmacy, 400347 Cluj-Napoca, Romania
- <sup>3</sup> Department of Internal Medicine, “Iuliu Hatieganu” University of Medicine and Pharmacy, 400347 Cluj-Napoca, Romania
- <sup>4</sup> École Centrale Nantes, Nantes Université, CNRS, LS2N, UMR 6004, F-44000 Nantes, France
- \* Correspondence: bogdan.gherman@mep.utcluj.ro

**Abstract:** This paper presents the development of the hardware and software architecture of a sixdegrees of freedom (DOF) parallel robot (PARA-SILSROB) by illustrating all the stages undertaken to achieve the experimental model of the robot. Based on the experimental model, the control architecture is also presented, which is primarily based on a master–slave control system through which the surgeon controls the robot using the master console composed of commercial peripheral components (two 3D Space Mouse devices, computer, and keyboard) integrated with the solution developed in this study and presented in this paper. The robot was developed also according to the surgical protocol and surgeon’s requirements, and for the functionality testing of the mechanical structure, two experimental stands were used. The first stand presented several surgical steps, such as manipulation, resection, and suture of experimental tissues (simulating real-life robot-assisted surgical maneuvers) using commercial instruments. The second stand presented a simulation of an esophagectomy for esophageal cancer and digestive reconstruction through a right intercostal approach. For this testing phase, the organs were created using 3D reconstruction, and their simplified models were 3D printed using PolyJet technology. Furthermore, the input trajectory generated using the master console was compared with the robot actuator’s movements and the obtained results were used for validation of the proposed robot control system.

**Keywords:** parallel robot; robot-assisted surgery; experimental test; surgical robot; esophagectomy; esophageal cancer; single incision laparoscopic surgery



**Citation:** Pisla, D.; Popa, C.; Pusca, A.; Ciocan, A.; Gherman, B.; Mois, E.; Cailean, A.-D.; Vaida, C.; Radu, C.; Chablat, D.; et al. On the Control and Validation of the PARA-SILSROB Surgical Parallel Robot. *Appl. Sci.* **2024**, *14*, 7925. <https://doi.org/10.3390/app14177925>

Academic Editors: Keri Kim, Ryu Nakadate, Jumpei Arata and Ayoung Hong

Received: 2 August 2024

Revised: 30 August 2024

Accepted: 3 September 2024

Published: 5 September 2024



**Copyright:** © 2024 by the authors. Licensee MDPI, Basel, Switzerland. This article is an open access article distributed under the terms and conditions of the Creative Commons Attribution (CC BY) license (<https://creativecommons.org/licenses/by/4.0/>).

## 1. Introduction

Open surgery (OS) or open approach remains the preferred technique in most surgical domains. It starts by making a significant incision that ranges from a few to several hundreds of millimeters to provide access to the desired organ(s). It provides high dexterity and a generous working space at the expense of a series of disadvantages ranging from the large size of the incision to prolonged hospitalization and recovery time because of the traumatic and invasive approach, which leads to an increased risk of postoperative complication and pain [1–3].

While open surgery was the preferred technique a few years ago, minimally invasive surgery (MIS) has undeniable advantages and has become the mainly used technique in high-volume centers. Even in oncological surgery, minimally invasive surgery has great advantages since it is safe, efficient, and assures the enhanced recovery of the patient [4].

The development of surgery in the last several decades has led to the broad adoption of minimally invasive techniques, which were first introduced in gynecology during the 20th century. This approach requires 3–5 incisions, each measuring between 5 to 15 mm. These incisions allow for the insertion of the necessary surgical instruments and typically include two active instruments: a laparoscopic camera and an aspiration tube [5–8]. Its benefits are numerous: reduced postoperative trauma, less intraoperative blood loss, improved cosmetic results due to smaller incisions, a shorter hospital stay, and faster recovery after surgery. However, even if it has proven advantages for the patient compared with OS, this method presents certain drawbacks for the surgeon, such as a reduced working space, decreased surgeon dexterity, narrower field of view, and the absence of tactile feedback [9].

The next-generation technique of minimally invasive surgery (MIS) is single-incision laparoscopic surgery (SILS). It implies a single incision, either at the navel or in the intercostal spaces, that ranges between 15 and 25 mm. Through this incision, two active instruments and a laparoscopic camera are introduced into the surgical field [10–12]. It provides several key advantages, including a single incision, a reduced hospitalization time of 1 to 3 days, minimal blood loss, decreased postoperative trauma, and good cosmetic results when the incision is made at the navel. The navel heals quickly since it is a natural embryonic opening and can conceal the incision effectively. This technique also comes with some notable disadvantages: an even more limited working space than in the laparoscopic approach; greater sensitivity to surgeon's hand tremors; abdominal pressure felt by the patient, which can lead to postoperative hernias; reduced surgeon's dexterity; and a long, steep learning curve [13,14]. The evolution from open surgery toward SILS is illustrated in Figure 1.

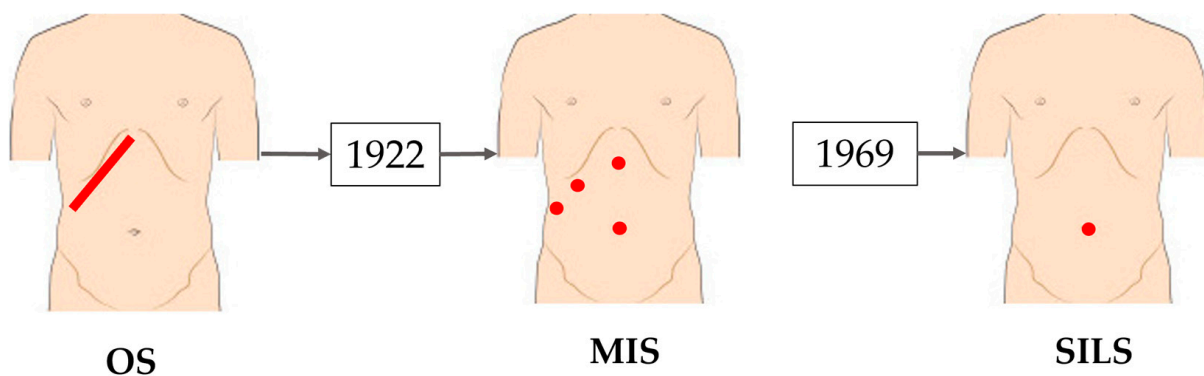


**Figure 1.** The evolution of surgery from classical surgery to single-incision laparoscopic surgery [15].

Due to their advantages and advancements, robots can now be utilized in various surgical procedures. The first robot employed in brain surgery was the PUMA robot in 1985. The foundation of robotic-assisted surgery was established between 1999 and 2000 with the commercial launch and FDA approval of the da Vinci robot by Intuitive Surgical [16–18]. The initial version of the da Vinci robot could manage up to four surgical instruments, including three active instruments and one laparoscopic camera. Its design featured four arms mounted on a console, and it was operated using the master–slave concept [19,20]. Additionally, this period saw the introduction of telerobotic surgery. The evolution of the da Vinci robots, alongside the improvements made to each structure, is illustrated in Figure 2 [21–25].

Although Intuitive Surgical currently dominates the market, the first significant competitor to the da Vinci system emerged in 2018 with the Senhance robot, which was developed by Asensus Surgical [26]. That same year, Intuitive Surgical received FDA approval for the da Vinci SP, which was the first robot dedicated to single-incision laparoscopic surgery (SILS) [27].



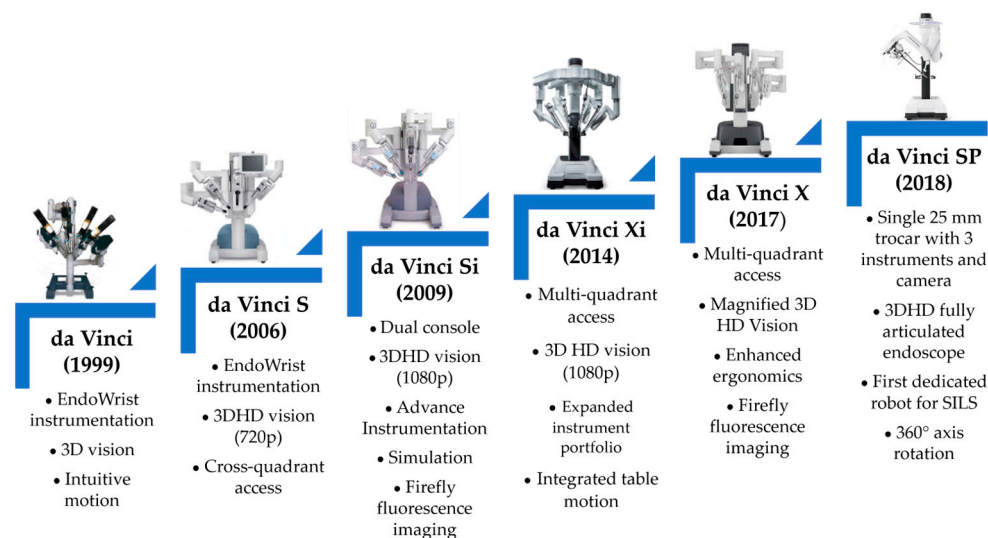


**Figure 2.** The evolution of the da Vinci robot [25].

Several other surgical robots are currently in development, as detailed in sources [28–31]. These include the Avatera, Bitrack, Hugo RAS System, Versius, Dexter, PARAMIS, Vicarious Surgical Robotic System, PARASURG 9M, and Hominis Surgical System.

These systems offer significant advantages over manual methods, thus greatly enhancing patient’s safety and the quality of surgical care. The benefits include eliminating the surgeon’s hand tremor, achieving increased precision, significantly improving surgeon ergonomics, eliminating the triangulation effect [32], scaling the surgeon’s hand movements, increasing the dexterity, simultaneously manipulating multiple instruments, and providing a 3D visualization of the surgical field with the option to use the firefly fluorescence imaging mode [33,34].

The primary disadvantages of these systems include high acquisition and operational costs, a steep learning curve for surgeons, potential collisions between robotic arms, limited workspace for instruments, extended setup and retrieval times in emergencies, and the lack of tactile feedback. The Senhance robot addresses some of these issues [33,34].

These robots are employed in various surgical procedures, including appendectomy, colectomy, cholecystectomy, gastric bypass, hernia repair, hysterectomy, pancreatectomy, and hepatectomy. Recent studies [35–38] demonstrated the use of robots with the SILS technique in complex surgeries, such as esophagectomy for esophageal cancer. These studies emphasized the role of robots in both the resection and reconstruction times of this surgical intervention by significantly reducing the patient’s trauma compared with the traditional methods [39]. Given the high difficulty and complexity of esophagus resection and reconstruction, along with the limited number of robotic systems available for such procedures, ongoing research and the development of new robotic systems and new techniques used to generate the path are essential for improved results in this field. The authors introduce several techniques for optimizing trajectory planning by utilizing neuro-fuzzy interference systems and redundant manipulators [40,41].

The current work presents the PARA-SILSROB parallel robot, which was developed for single-incision laparoscopic surgery, where its control system and initial laboratory experimental tests were used in the first phase of the Ivor–Lewis esophagectomy procedure [42]. PARA-SILSROB offers significant advantages over current solutions, particularly the da Vinci SP, including enhanced stiffness in both the mobile platform (which supports the active instruments) and the surgical instruments themselves, as well as improved ergonomics, which makes it easier to mount and dismount the active instruments. In comparison with the Senhance, PARA-SILSROB utilizes a single mobile platform that houses the active instruments, which results in a more compact design and a reduced footprint in the operating room.

This paper is structured as follows: Section 2 presents the surgical protocol used to test the experimental model of the PARA-SILSROB parallel robot. This section continues with a description of the experimental model of the robot, the command-and-control architecture of the robot, and the presentation of the graphical interface designed for both the surgeon and the engineer, who monitor the system’s operation during surgery. Section 3 describes the experimental tests conducted with the PARA-SILSROB parallel robot under laboratory conditions using two training setups designed for SILS. Sections 4 and 5 present the discussions and conclusions of this work.

## 2. Materials and Methods

### 2.1. Experimental Model of the Parallel Robot PARA-SILSROB

The parallel robot PARA-SILSROB was developed based on the medical protocol [3] and the requirements set forth by surgeons [43].

This robot was developed in accordance with the master–slave concept and this chapter focuses on presenting the architecture of the robotic system, beginning with the kinematic scheme and concluding with the mechanical assembly.

The development stages of the experimental model are illustrated in Figure 3 (kinematic scheme of the robot), Figure 4 (3D design of the robot), and Figure 5 (experimental model of the robot).

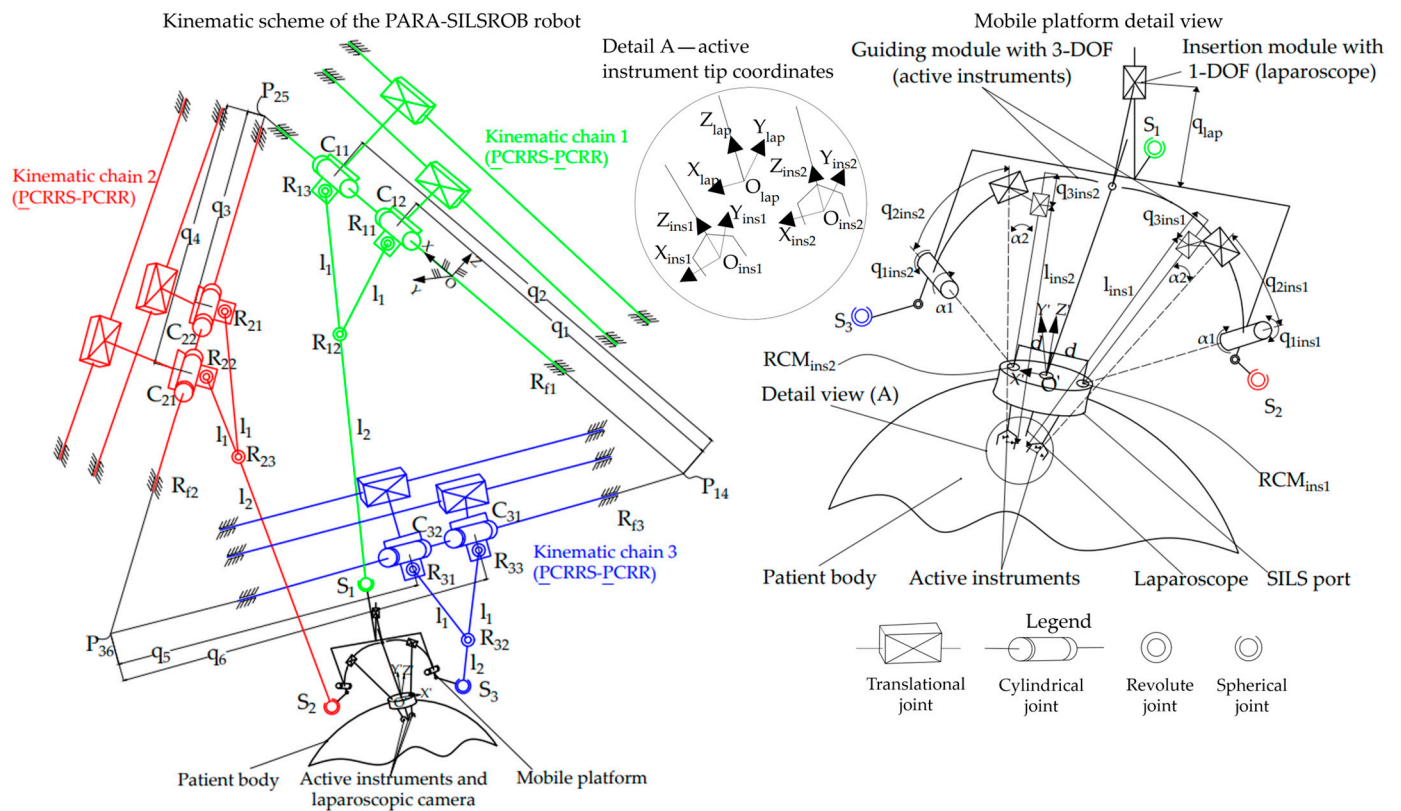


Figure 3. The kinematic scheme of the PARA-SILSROB robot.

The kinematic scheme of the robot was defined, presented, and detailed in [20], and resulted in a parallel structure of the type  $3\text{-PCRRS-PCRR}$ , which consists of 3 identical kinematic chains mounted on a triangular frame. The next stage in the development of the parallel robot involved designing the 3D model based on the kinematic scheme detailed in [3]. The final stage consisted of assembling the mechanical structure using the information obtained from the first two stages (the kinematic scheme and the 3D design).

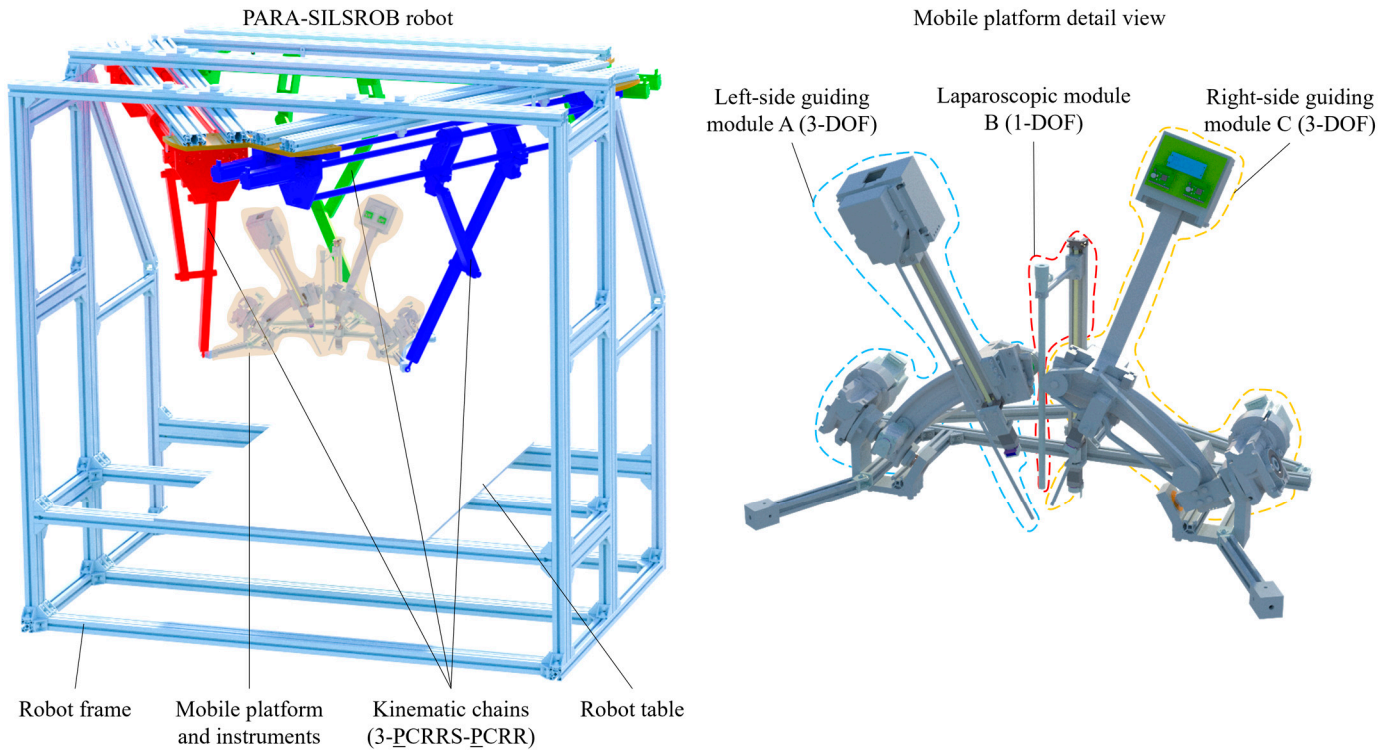


Figure 4. The 3D design of the PARA-SILSROB robot.

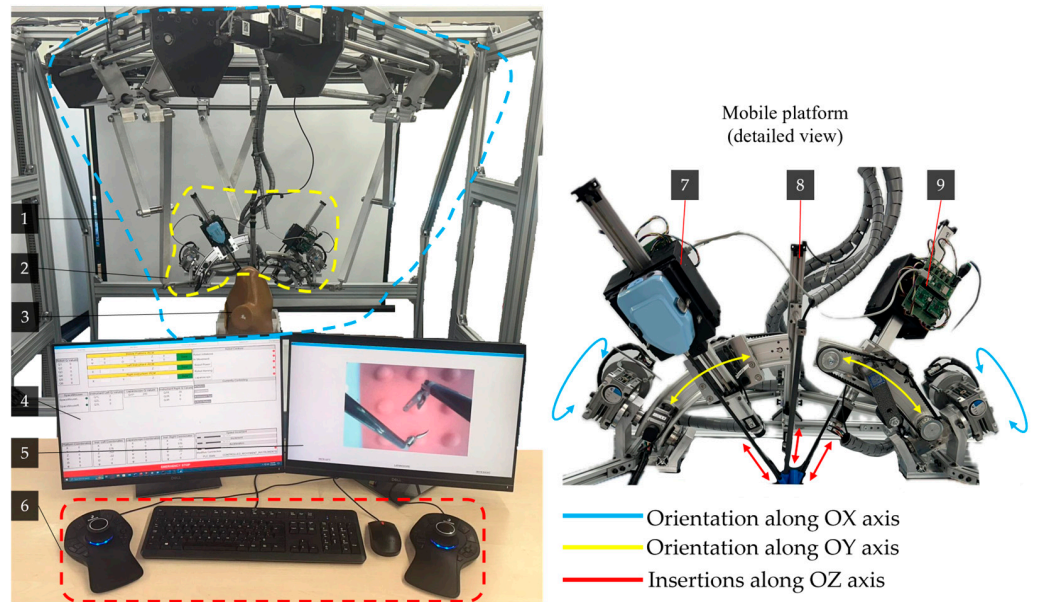


Figure 5. Experimental model of the PARA-SILSROB robot including the main components and the movements of the serial modules: (1) PARA-SILSROB; (2) Mobile platform; (3) Torso training; (4) Graphical user interface for engineers; (5) Graphical user interface for surgeons; (6) 3D Space Mouse devices with keyboard and mouse; (7–9) Serial modules used for instrument handling).

The kinematic scheme shown in Figure 3 illustrates the three identical kinematic chains ( $KC_i, i = 1..3$ ) and provides a detailed view of the mobile platform (MP) of the PARA-SILSROB robot. The fixed coordinate system (OXYZ) is positioned on the first kinematic, which consists of two active translational joints ( $q_1, q_2$ ) connected by two cylindrical joints ( $C_{11}, C_{12}$ ). One cylindrical joint serves the main link (denoted as  $l_1 + l_2$ —the length between the revolute joint  $C_{11}$  and the spherical joint  $S_1$ ), while the other serves the secondary



link (denoted as  $l_1$ —the length between the revolute joint  $C_{12}$  and the revolute joint  $R_{12}$ ). Additionally, the chain includes four passive revolute joints ( $R_{f1}$ ,  $R_{11}$ ,  $R_{12}$ ,  $R_{13}$ ) and a passive spherical joint ( $S_1$ ), which connects the kinematic chain to the mobile platform. The structural synthesis analysis of the PARA-SILSROB robot is detailed in [20], which means that the system has six degrees of freedom (6-DOF). This capability allows for the manipulation and orientation of instruments along the three axes ( $OX$ ,  $OY$ ,  $OZ$ ).

The active instruments and the laparoscope are mounted on the mobile platform of the PARA-SILSROB robot using three serial modules. Two of these modules each provide 3-DOF for the orientation and insertion of the active instruments (two active revolute joints for the left and right module denoted as  $q_{1ins1}$  and  $q_{1ins2}$ , and four active prismatic joints denoted as  $q_{2ins1}$  and  $q_{3ins1}$  for the left module and  $q_{2ins2}$  and  $q_{3ins2}$  for the right module). Additionally, there is a third module with 1-DOF dedicated to the insertion of the laparoscope (denoted as  $q_{lap}$ ). These modules were specifically designed to ensure that the RCMs (remote centers of motion) of the instruments are architecturally constrained, which is a critical feature for robotic-assisted surgery [44].

Figure 4 illustrates the 3D CAD model of the PARA-SILSROB robot and a detailed view of the mobile platform. The modeling was performed using the Siemens NX software program (Version 12 provide by Siemens PLM Software, founded in 1963 in Torrance, CA, USA, country Germany, Office Plano, TX, USA) [45].

Figure 5 illustrates the development stage of the experimental model of the PARA-SILSROB robot (1), which features a detailed view of the mobile platform (2) and torso training (3). This control architecture includes two graphical interfaces (4 graphical interfaces for the engineer and 5 graphical interfaces for the surgeon).

The surgeon operates the robot (slave) using a keyboard and two commercially available 3D Space Mouse devices (6), which are integrated into the command-and-control logic detailed in Section 2.2. The figure also illustrates the movements of the three serial modules (7, 8, 9) attached to the mobile platform. These modules are used for orienting and inserting the active instruments, which are commercial products developed by Intuitive Surgical, as well as the laparoscopic camera. These motions are achieved through seven actuators attached to the mobile platform (three for modules A and C, and one for module B). Additionally, the training simulator kit used for the experimental tests is shown in the figure. At this stage of the robot's development, the active instruments used are commercial models for which custom mounting brackets and tip control mechanisms were designed using two printed circuit boards (PCBs). These boards control the actuators (four per active instrument) that manipulate the tips of the active instruments. A more detailed explanation of these components can be found in [46] and in the next subsection.

## 2.2. Command and Control Architecture of the Parallel Robot PARA-SILSROB

The command-and-control system integrates both hardware and software components, which allows it to execute the surgeon's commands and convert inputs from peripherals (3D Space Mouse devices, version Space Mouse Pro, developed by 3DConnexion, Munich, Germany, 2001) into controlled movements. The master–slave architecture is used to restrict the robot's ability to move autonomously. Safety measures [47] are implemented through hard limits configured within the software part of the system and through signals that are either tied to mechanical emergency buttons or graphically represented in the graphical user interface (GUI).

The robustness and low cycle times of an industrial-grade programmable logic controller (PLC) proved adequate for this purpose. This capability allows the control system to be easily scaled to accommodate additional actuators, sensors, and other devices as needed. Consequently, it provides the necessary resources for future developments while ensuring that the existing functionalities remain intact.

### 2.2.1. Hardware Architecture

The hardware configuration of the command-and-control architecture of the parallel robot is organized into three levels, as illustrated in Figure 6. At the user level, input data is transmitted to the command-and-control level, which is responsible for the processing, conversion, and transmission to the physical level of the robot [48].

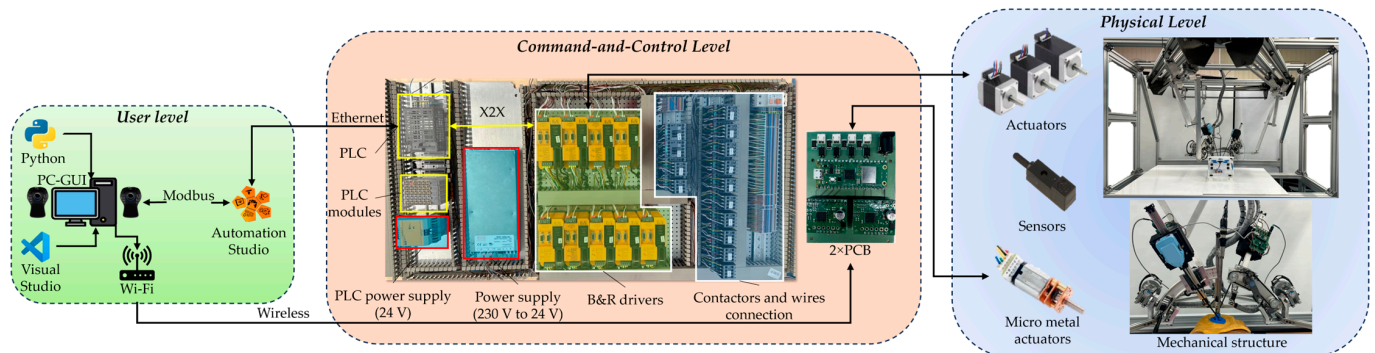


**Figure 6.** Hardware configuration of the PARA-SILSROB.

For the control system, a PLC from Bernecker and Rainer Industrial Automation (B&R) is used, specifically the X20CP3586 model, which was selected for its low cycle time of 100  $\mu$ s. The driver modules are also from B&R, specifically the 80SD100XD.C044-01, which accommodates two actuators at a time. The configuration consists of 18 actuators, 13 of which are managed by 7 B&R drivers that control the kinematic chains and the three modules attached to the mobile platform. An additional 8 actuators are linked to four drivers that are directly connected to the PCBs shown in Figure 6 and are responsible for controlling the tips of the active instruments. The connection between the drivers and the PLC is achieved via X2X, which requires the use of an additional module, namely, a X2X link bus transmitter from B&R named X20BT9100, which was designed for X20 systems to facilitate seamless expansion. The encoders, homing sensors, and potential brakes are connected directly to the drivers. A comprehensive overview of the entire hardware configuration system is presented in Figure 6.

### 2.2.2. Software Architecture

Bernecker and Rainer Industrial Automation (B&R) provides specialized software for their hardware solutions called Automation Studio (Version 4.12, Company B&R, Eggelsberg, Austria, 2001). This software integrates the configuration and programming of their devices, which facilitates a streamlined approach to automation.

In this setup, a state machine was implemented to execute commands based on input data transmitted from peripheral equipment (two 3D Space Mouse devices, keyboard, and mouse) and the data collected from the robotic system. Several other programs are designed to run concurrently, thus providing the state machine with the necessary data to effectively manage the robotic system. Figure 7 illustrates the software control scheme, thus showcasing all the elements involved in this configuration.

The bundled states handler encodes the data into a simplified representation of the robotic system and inputs it into the state machine once the actuator's parameters have been obtained. Another software module, which is known as the Modbus Handler, provides the management of signal and data reading and writing between the robot and the GUI. The state machine utilizes the inverse and direct kinematics model [20] based on the given user inputs. The model integrates the actuator parameters and user input through a 3D Space Mouse control device to generate the necessary velocity vectors. These velocity vectors are then transmitted to the speed and direction handler. The function of this handler is to establish the new parameters for each actuator based on the calculated velocity and direction.



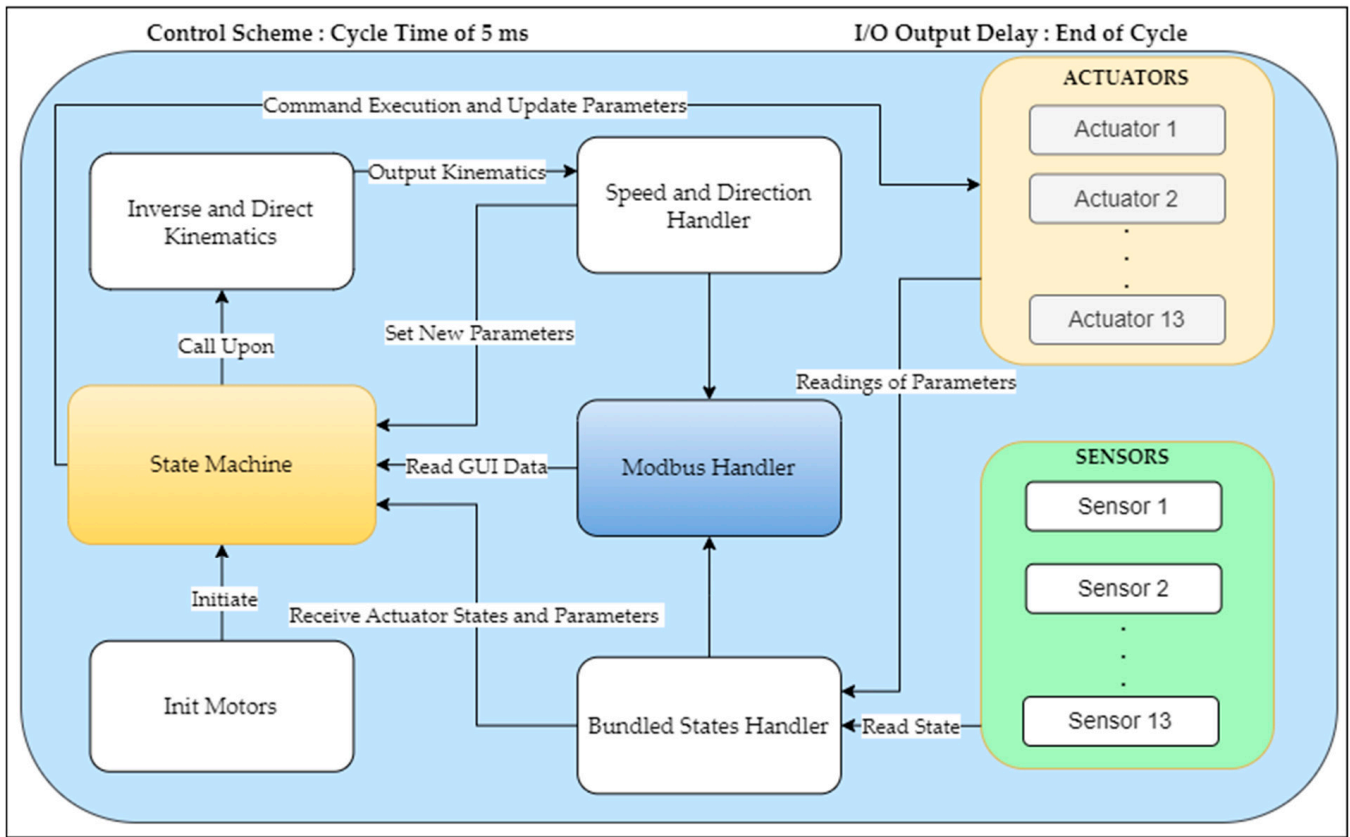
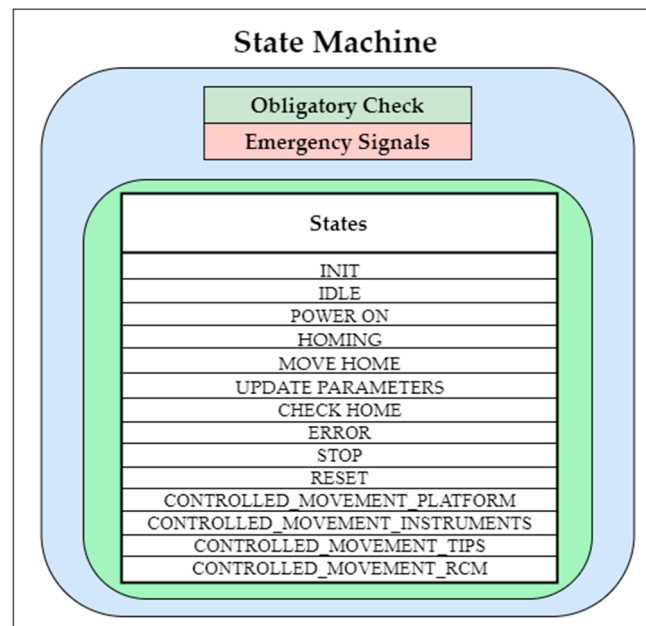


Figure 7. Software configuration of the PARA-SILSROB.

This structured approach facilitates the systematic control and monitoring of the robotic structure, which ensures efficient operation. For a more comprehensive understanding of the various states of the state machine, please refer to Figure 8a,b.



(a)

Figure 8. Cont.

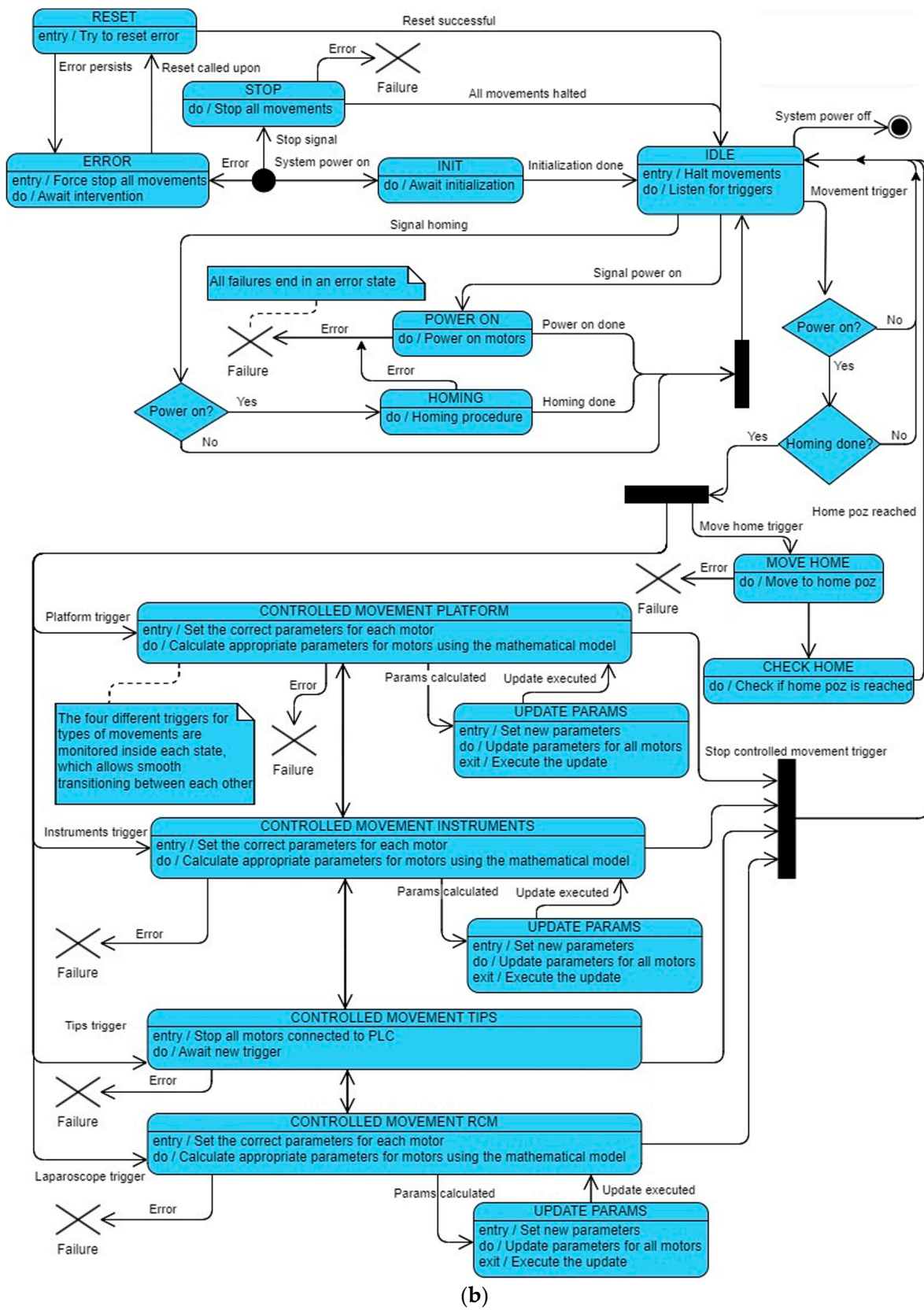


Figure 8. (a) PARA-SILSROB robot state machine and (b) PARA-SILSROB robot state machine block diagram.

According to Figure 8a,b, the initial state “INIT” is the state, which is automatically activated when the robot is powered on. This transition occurs from the POWER\_ON state, which is accessed from the IDLE state, which is recognized as the robot’s default state. From this initialization, the HOMING state is activated to execute the homing instruction for the entire robotic system. The CONTROLLED\_MOVEMENT\_PLATFORM can be accessed from various states, including IDLE and other CONTROLLED\_MOVEMENT states. It enables the application of inverse kinematics [20], which allows for the precise manipulation of the end effector’s movement in three-dimensional space, as driven by the input from the 3D Space Mouse. The 3D Space Mouse transmits data using the Modbus protocol. The CONTROLLED\_MOVEMENT\_INSTRUMENTS state applies inverse kinematics [20] as well, but it restricts itself to a limited number of actuators for positioning the instruments, as depicted in Figure 5. Finally, the CONTROLLED\_MOVEMENT\_TIPS refers to a state where the use of all 18 actuators is halted and the control is transferred to the two Raspberry PI Pico boards mounted on the two PCBs, which are located inside the instrument casings (one PCB for each casing). These Pico boards manage four actuators each and utilize four drivers (two drivers for one PCB) and a power supply. These actuators provide the two instrument tips with the freedom to adjust and grasp as needed. Within the state machine, the CONTROLLED\_MOVEMENT\_RCM state is dedicated to the precise positioning of the laparoscope camera in three-dimensional space once it has been inserted. This state utilizes inverse kinematics [20] for the movement control, which allows for rotations limited along the X- and Y-axes. In terms of safety, the STOP state can be activated solely by pressing an emergency button. This feature is designed for the rapid cessation of the drivers’ operation, which enables the robot to halt smoothly through deceleration. Upon clearing the emergency button, the system transitions back to the IDLE state unless an error is detected. Additionally, the state machine is equipped to handle rectifiable errors, such as speed or position discrepancies, which allows it to recover from minor uses effectively without requiring a system restart.

### 2.3. Graphical Interface of the Parallel Robot PARA-SILSROB

To interact with the robotic structure, a user-friendly GUI was developed. This interface was designed to integrate and display relevant data from the PLC regarding the laparoscope and the active instruments. Two main GUIs were developed: the surgeon’s view presented in Figure 9 and the engineer’s view illustrated in Figure 10.

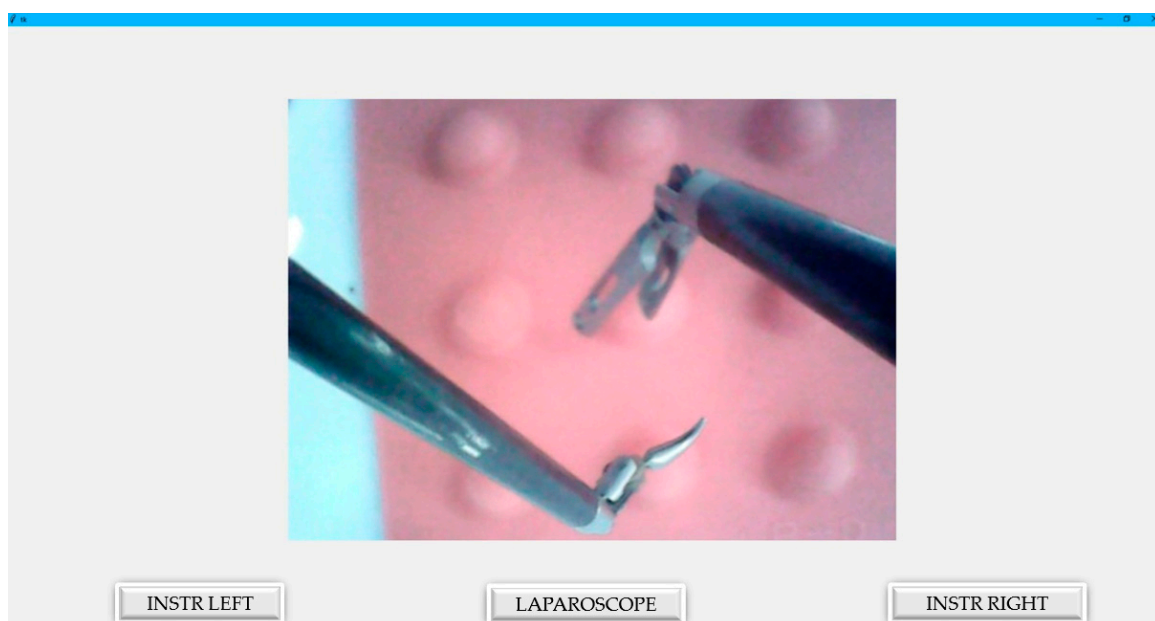


Figure 9. Graphical user interface for the surgeon.

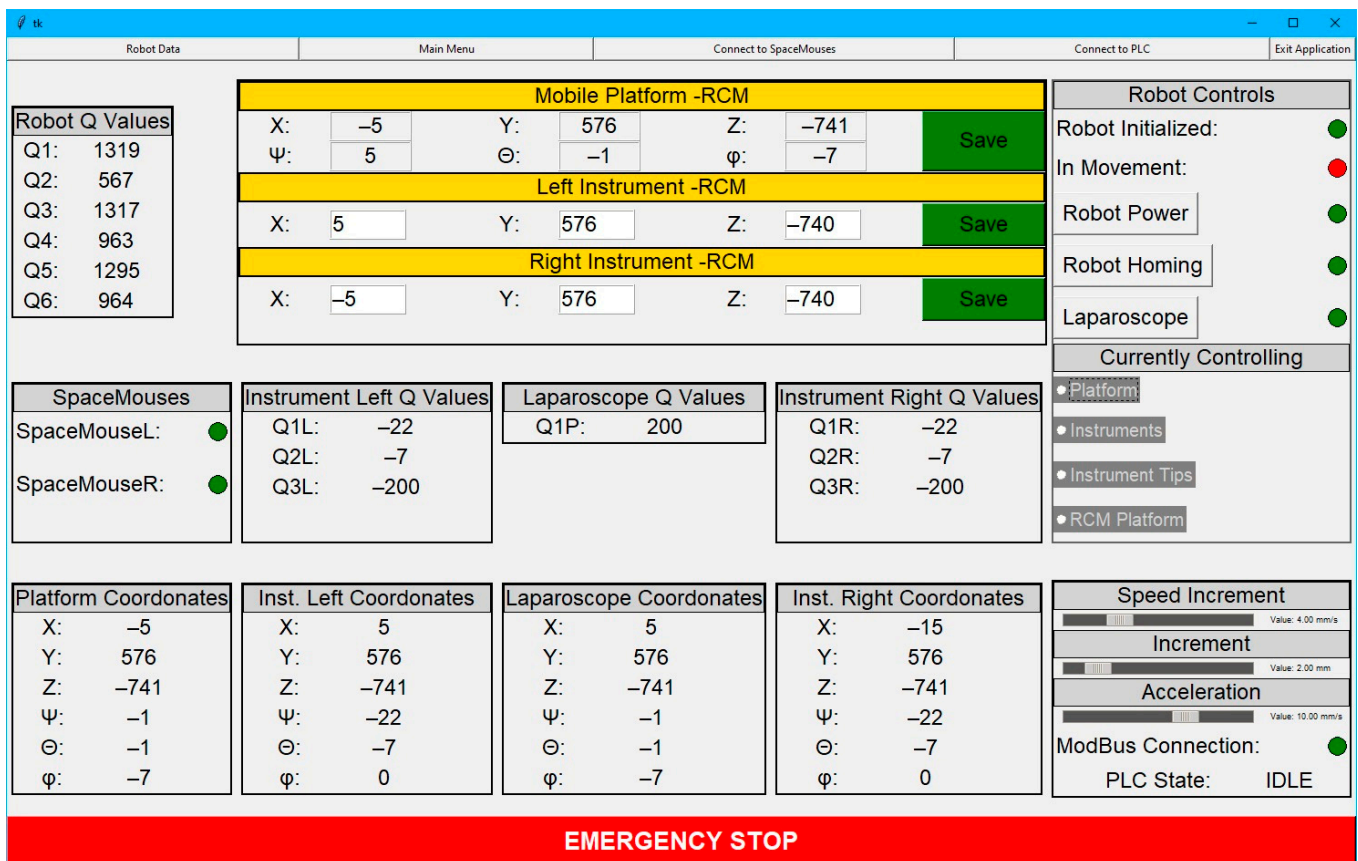


Figure 10. Graphical user interface from the engineer's view.

The surgeon's GUI is defined by its simplicity, as it displays only what is relevant, without cluttering the screen with unnecessary data. Moreover, it shows the image generated by the laparoscope within the intraoperative field. Thanks to the simplified interface and the robot's command console, surgeons are expected to adapt easily to the working environment. The interface, which consists of only three buttons, significantly enhances the user-friendliness of PARA-SILSROB. Additionally, the system integrates two commercial 3D Space Mouse devices, which feature several configurable buttons, thus offering greater flexibility compared with commercial systems that require surgeons to adapt to a predefined mode of operation. These devices, which are used for controlling the robot, are equipped with a central controller head with 6-DOF and are designed to be intuitive, with a coordinate system that is parallel to that of the robot. Another advantage is that these devices, which are integrated into the command console, do not require repositioning. This contrasts with traditional robotic-assisted surgery consoles, which necessitate repositioning using pedals or additional buttons on the master console.

The graphical interface shown in Figure 10 is designed specifically for engineers to facilitate real-time monitoring and management of the robot, the mobile platform, the active instruments, and the laparoscope. The interface also features a series of buttons to change the robot's operating states and provide real-time status updates on the robot's functionality.

### 3. Results

#### 3.1. Medical Protocol Used for Experimental Tests

The experimental tests of the PARA-SILSROB parallel robot were conducted in adherence to the medical protocol developed in collaboration with medical experts, as outlined in [43]. Based on this protocol, Table 1 presents a comprehensive overview of the procedures used to evaluate the robot's experimental model, which encompasses both technical and medical tasks.



**Table 1.** Medical protocol used to perform the experimental tests with the PARA-SILSROB in a laboratory.

Procedure's Steps	Technical Tasks	Medical Tasks
Step 1 Preplanning	<ul style="list-style-type: none"> <li>• Testing the functionality of the robot;</li> <li>• Sending the robot to homing position;</li> <li>• Performing preoperative simulation;</li> <li>• Testing the instrument's tips;</li> <li>• Testing the functionality of the master console.</li> </ul>	<ul style="list-style-type: none"> <li>• Checking the patient's medical history;</li> <li>• Establishing the surgical approach and medical management;</li> <li>• Advanced medical imaging;</li> <li>• 3D reconstruction of the target organ and visualization using augmented reality (AR) [49].</li> </ul>
Step 2 Environment configuration	<ul style="list-style-type: none"> <li>• Attaching the laparoscope and positioning it in the center of the mobile platform;</li> <li>• Initializing the homing procedure.</li> </ul>	<ul style="list-style-type: none"> <li>• Attaching the testing stand on the robot table;</li> <li>• Simulating the incision and inserting the SILS port;</li> <li>• Attaching the models in the training kit used for testing the functionality of the robot.</li> </ul>
Step 3 Mobile platform positioning and orientation	<ul style="list-style-type: none"> <li>• Positioning the mobile platform and the tip of the laparoscope above the insertion points;</li> <li>• Saving the point above the insertion point;</li> </ul>	<ul style="list-style-type: none"> <li>• Confirming the visual position and preparing the instruments.</li> </ul>
Step 4 Laparoscope insertion and RCM [44] saving point	<ul style="list-style-type: none"> <li>• Inserting the laparoscope and saving the RCM (remote center of motion) point inside the trocar.</li> </ul>	<ul style="list-style-type: none"> <li>• Manually inserting the active instruments and attaching them to the modules of the mobile platform, under laparoscope control</li> </ul>
Step 5 Active instruments insertion	<ul style="list-style-type: none"> <li>• Attaching and fixing the active instruments to the orientation modules of the mobile platform;</li> </ul>	<ul style="list-style-type: none"> <li>• Monitoring the process of instrument insertion.</li> </ul>
Step 6 Performing the surgical procedure	<ul style="list-style-type: none"> <li>• Controlling modules of the instruments through the master console;</li> <li>• Reorienting the laparoscope by compensating for the movement of the active instruments [50].</li> </ul>	<ul style="list-style-type: none"> <li>• Preparing the instruments necessary for the medical procedure and replacing the active instruments as needed;</li> <li>• Safety measurements for surrounding organ unseen lesions during procedure.</li> </ul>
Step 7 Surgical procedure ending	<ul style="list-style-type: none"> <li>• Surgical instruments retraction in RCM points;</li> <li>• Moving the robot to a safety position;</li> <li>• Visually inspecting the mechanical structure of the robot and the master console;</li> <li>• Generating a report and collecting the messages that appeared during the medical procedure, shutting down the entire system, and disconnecting it from the power supply.</li> </ul>	<ul style="list-style-type: none"> <li>• Detaching and removing the laparoscope and active instruments from the surgical field;</li> <li>• Removing the testing kit from the robot table;</li> <li>• Sterilizing the instruments used during the surgical procedure.</li> </ul>

The medical testing procedure for the PARA-SILSROB robot presented in this study is based on the application of robot-assisted minimally invasive surgery during the first step of the Ivor–Lewis esophagectomy procedure [36]. This procedure comprises two distinct steps: the initial step uses an abdominal approach, while the subsequent step uses a right thoracic intercostal approach. The robot's testing plan was specifically tailored to the first step, which includes a series of maneuvers, such as tissue manipulation and dissection, resection, and ligation, as well as preparation for step two, which involves the reconstruction or eso-gastrostomy and anastomosis between the esophageal stamp and the stomach advanced into the thorax.

### 3.2. Experimental Tests of the Parallel Robot PARA-SILSROB In Laboratory Conditions Based on Medical Protocol and Surgeon's Requirements

The PARA-SILSROB parallel robot underwent experimental testing in a laboratory environment using two distinct test stands to assess the functionality of the robot's me-



chanical structure. The first stand consisted of a simulation and training kit designed for laparoscopic applications, while the second stand featured a torso that housed the target organ, the esophagus. This organ was generated using 3D printing techniques based on a 3D reconstruction derived from images produced by a helical CT scanner.

### 3.2.1. Testing the PARA-SILSROB Robot Using the Simulation and Training Kit Used for a Laparoscopy

During the test stage, three training modules were used and they were placed inside the simulation and training kit used for laparoscopy. Based on these training modules, the following operations were performed:

- Handling the plastic kit elements within the intraoperative field;
- Manipulating and resection of tissue;
- Simulating tissue suturing procedures.

To perform the previously described operations using the PARA-SILSROB robot, it was essential to first move the robot to its homing position. Subsequently, using the master console (as detailed in Section 2.2), the robot was positioned above the designated insertion point. This procedure relied on real-time data transmitted to the master console by the laparoscope attached to the mobile platform. Following the positioning, the laparoscope was inserted into the intraoperative field, and its RCM point was recorded. The attachment and insertion of the active instruments into the orientation and insertion modules were performed manually (Figure 11).

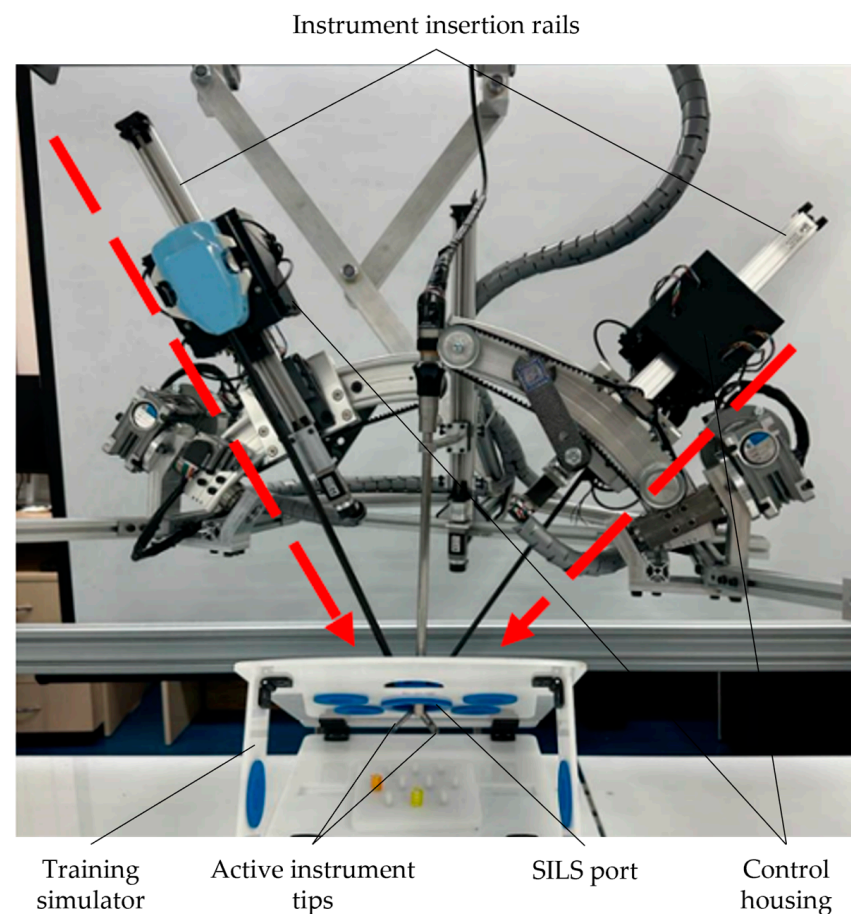


**Figure 11.** Active instruments developed by the Intuitive Surgical used for performing the insertion into the laparoscopic training kit.

During the manipulation stage, which involved plastic springs within the intraoperative field, two commercial active instruments, each with a diameter of 8 mm, were used,

alongside a laparoscope with a diameter of 10 mm. All instruments were inserted through the SILS port in the training simulator.

The results from this stage are presented in Figure 12, which shows the arrangement of the plastic springs on the plastic training module. This module was also equipped with a set of plastic rods.

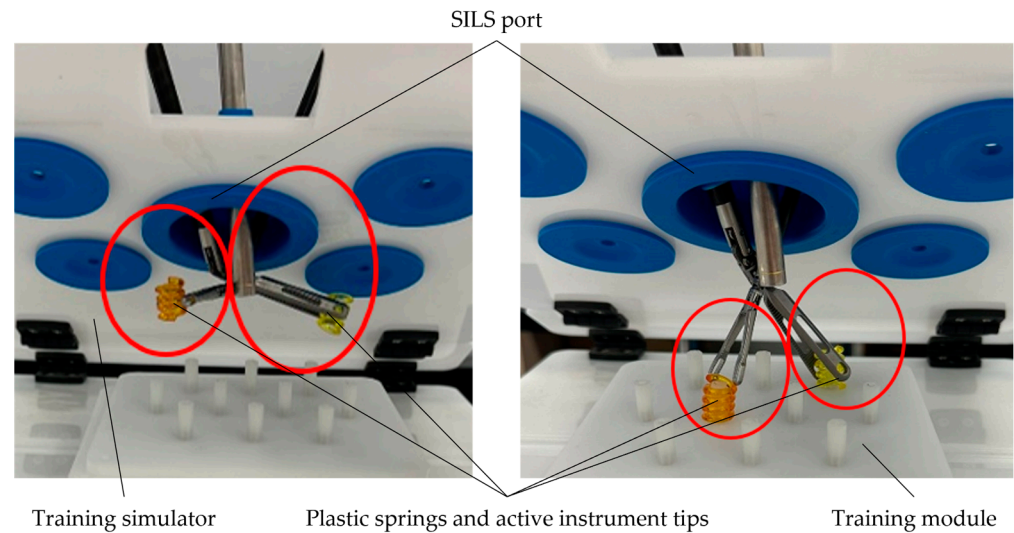


**Figure 12.** Manipulation stage of the plastic springs.

During the manipulation stage, which involved putting a cable through the rings, two commercial active instruments with an 8 mm diameter, which were equipped with articulated tips, were used, alongside a 10 mm laparoscopic camera. The outcome of this stage is illustrated in Figure 13.

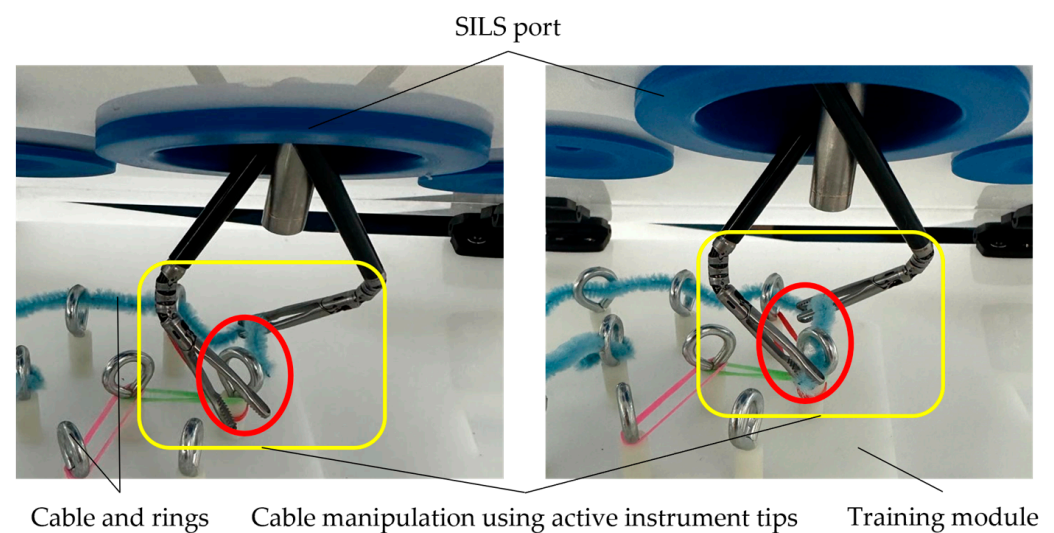


**Figure 13.** Cable manipulation using the training module with rings.

During the simulation of the tissue-cutting stage, a silicone module was used. This stage involved the use of an 8 mm diameter articulated tip active instrument for tissue grasping, an 8 mm diameter curved scissor-type active instrument, and a 10 mm diameter laparoscopic camera. The outcome of this stage is illustrated in Figure 14.

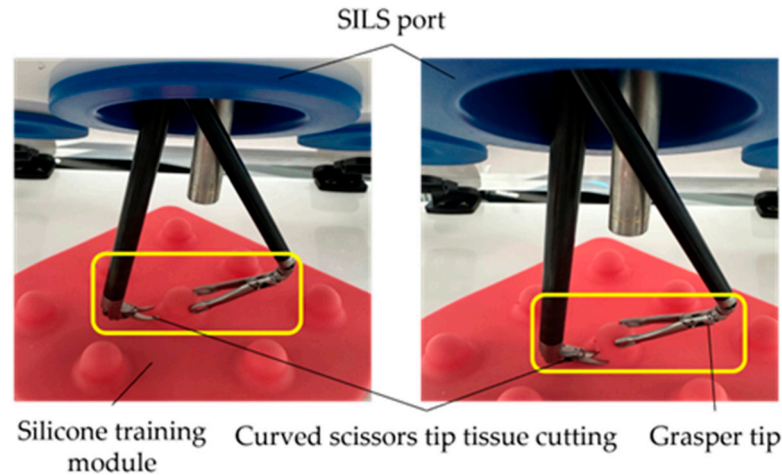


**Figure 14.** Tissue cutting stages simulation using a silicon module.

The final stage of this testing phase of the PARA-SILSROB robot involves simulating tissue suturing. For this operation, two commercial active instruments (EndoWrist large needle driver and EndoWrist flexible grasper, developed by Intuitive Surgical, Sunnyvale, CA, USA, 2014), both with an 8 mm diameter, along with a 10 mm diameter laparoscope, were used. The outcome of this stage is illustrated in Figure 15.

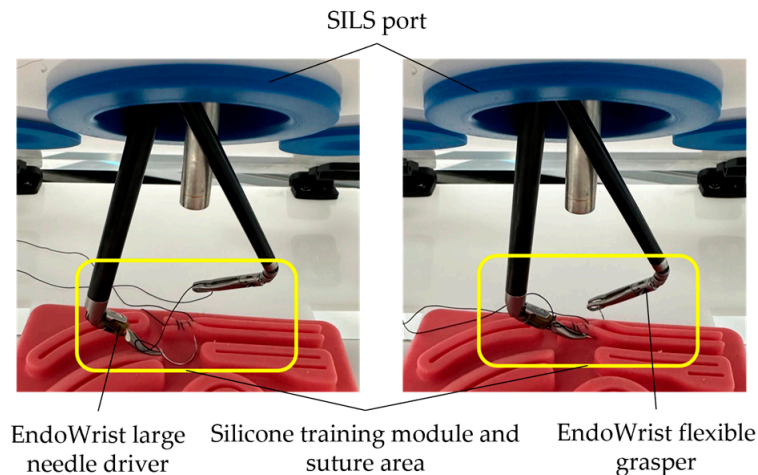


**Figure 15.** Simulating the suturing stage using a silicone training module.

### 3.2.2. Testing the PARA-SILSROB Robot Using a Torso with the Target Organ

In this stage, the simulation of an esophagectomy and digestive reconstruction procedure is presented. A torso that housed the esophagus and nearby organs (aortic arch with the descending aorta, superior and inferior vena cava, trachea) was used for testing the PARA-SILSROB robot. To generate the target organ (esophagus), 3D reconstruction was performed using computed tomography (CT) images. An analysis of the surfaces was carried out with the 3D Slicer software, which resulted in the 3D model shown in Figure 16a. The 3D reconstructed organs (Figure 16a) were simplified, followed by modeling and printing using PolyJet 3D printing technology (MediJet J5 3D printer, developed by Stratasys, Eden Prairie, MN., U.S., [51]), which is a technology that allows for printing organs with soft materials. The result of the 3D simplified model is illustrated in Figure 16b. The simplified model of the organs used in this phase may influence the results and their accuracy due to the lower level of complexity and the absence of neighboring organs. However, for this stage of robot testing, this simplified version was validated by experts in the field, and the model was approved for conducting these experimental studies. For the next testing phase and after analyzing the results obtained from these experiments, areas



where improvements can be made to both the organs and the approach used with the robot presented in this paper will be reviewed and considered.

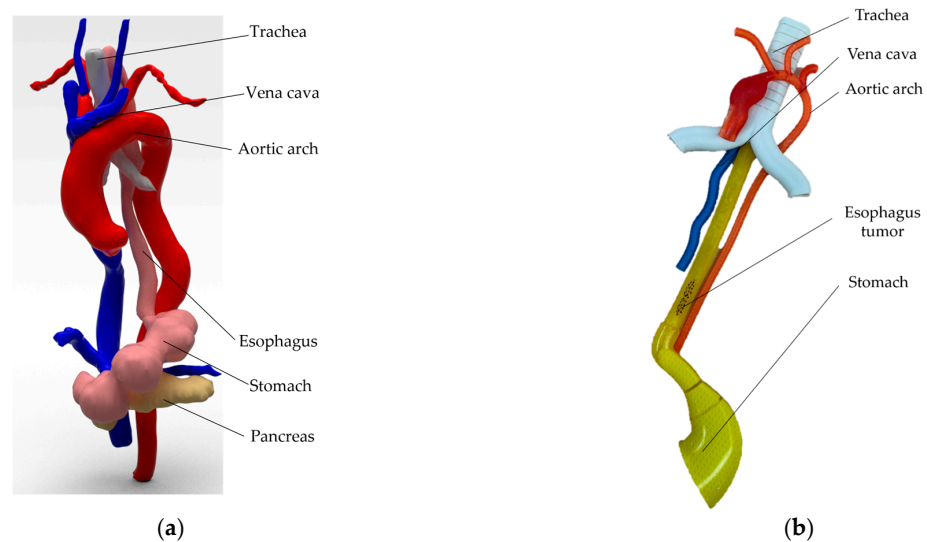


**Figure 16.** The virtual and 3D printed model of the esophagus (the 3D model of the real organs generated based on the 3D reconstruction is shown in (a), (b) represented the simplified 3D printed model of the organs using 3D printing technology).

To replicate the surgical environment for tumor resection on the 3D-printed esophagus, the esophagus was placed inside a torso positioned on the PARA-SILSROB robot's table. The SILS port was securely integrated into the torso, which allowed for the introduction of active instruments and a laparoscope through this access point. The intervention presented in this subsection focused on the thoracoscopic procedure, specifically on esophageal resection and reconstruction via a right intercostal approach. During this stage, the patient was positioned in the left lateral decubitus. The complete setup used for this procedure is illustrated in Figure 17.

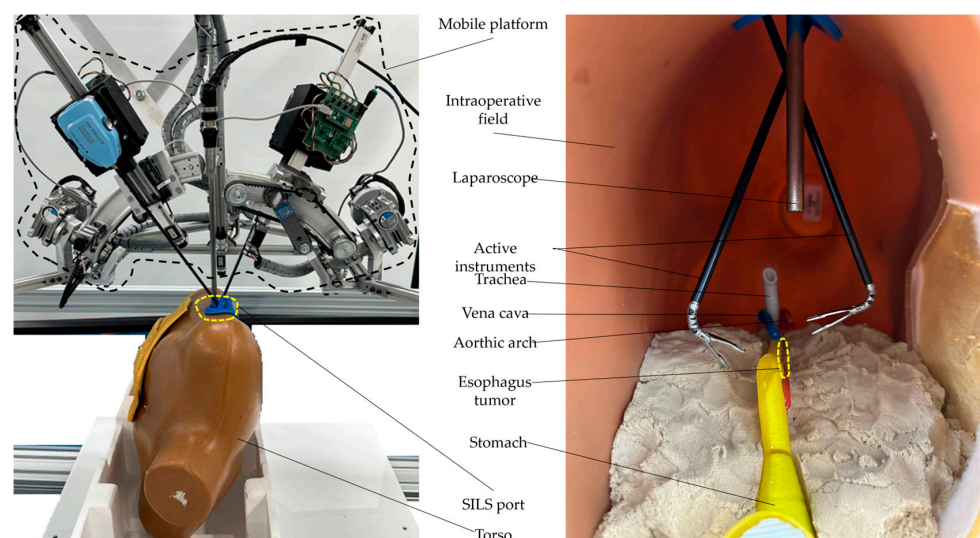


**Figure 17.** Experimental setup with the esophagus placed inside the torso.

The following steps outline the simulation of tumor resection in the lower esophagus under laboratory conditions using the PARA-SILSROB robot:

- Initialization of the homing procedure and functionality testing of all PARA-SILSROB robot components.

- Securing the torso with the 3D-printed esophagus on the PARA-SILSROB robot's table.
- Positioning the mobile platform with the laparoscope above the designated insertion point and inserting the laparoscope into the torso (laparoscope RCM saved).
- Attaching and inserting the commercial active instruments used for medical procedures (one 8 mm thoracic grasper and one 10 mm linear stapler).
- Performing the resection procedure and suturing the esophagus.
- Retracting the active instruments and laparoscope from the intraoperative field.
- Moving the robot to a safe position and completing the simulation by removing the port from the torso.

The results of these steps are illustrated in Figures 18–21.

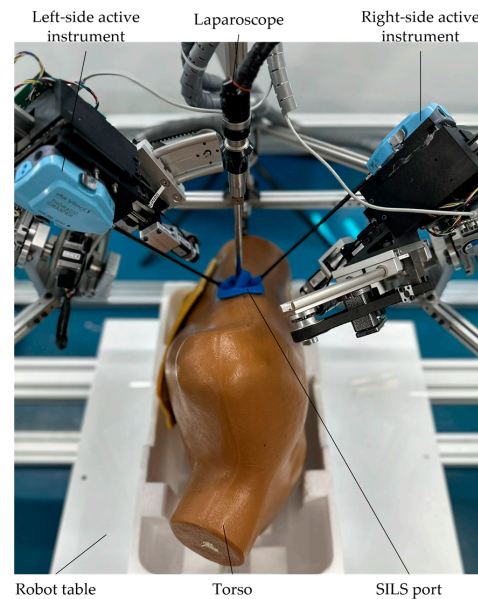


**Figure 18.** Laparoscope and commercial active instruments insertion into the torso.



**Figure 19.** Tumor resection preparation using an active instrument and a linear stapler.



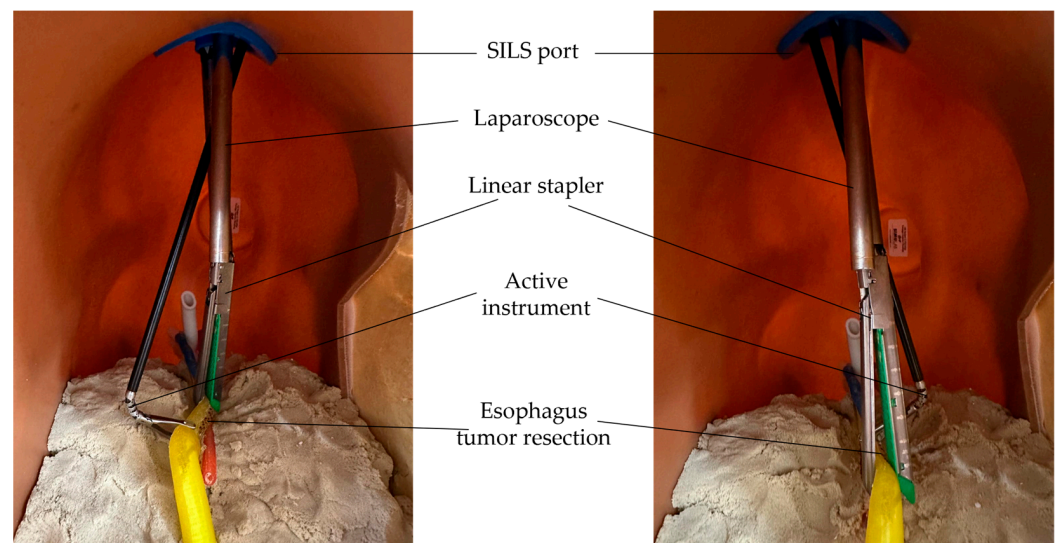


**Figure 20.** Simulating the resection of esophagus tumor using a linear stapler.

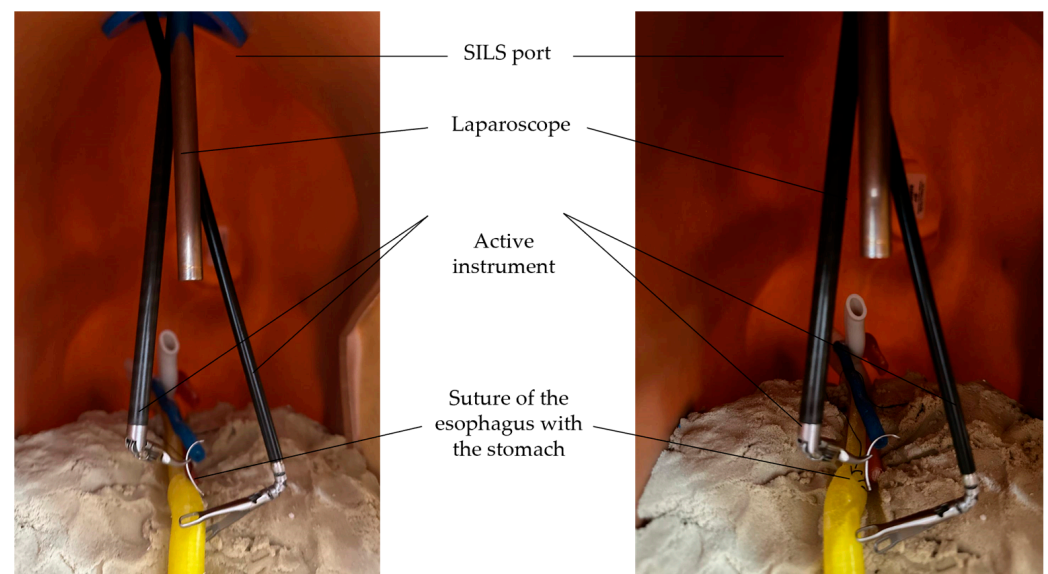


**Figure 21.** Simulating the suture of the esophagus with the stomach.

The time history diagram of the laparoscope tip velocities for the procedure presented in the previous figures was generated ( $\dot{X}_E, \dot{Y}_E, \dot{Z}_E, \dot{\psi}, \dot{\theta}, \dot{\varphi}$ ) using both inverse and direct kinematic models [20]. The input data for these graphs were collected from the master console during the medical procedure and include velocity vectors related to motion along and around the axes (encompassing both linear and angular velocities). These velocities were used to determine the positions of the laparoscope tip, which, in turn, were further used to determine the inverse kinematic model, thus yielding the displacements and velocities ( $q_1, \dots, q_6$  and  $\dot{q}_1, \dots, \dot{q}_6$ ) of the active joints. Furthermore, the motors' positions were determined through the encoders' signals, and their values served as input for the direct kinematic model to derive the robot's actual motion trajectory, which included the displacements and velocities. This actual trajectory was then compared with the theoretical trajectory. The graphs representing these results were generated using MATLAB software (developed by MathWorks, founded in Portola Valley, CA, U.S, 1984) and are illustrated in Figure 22.

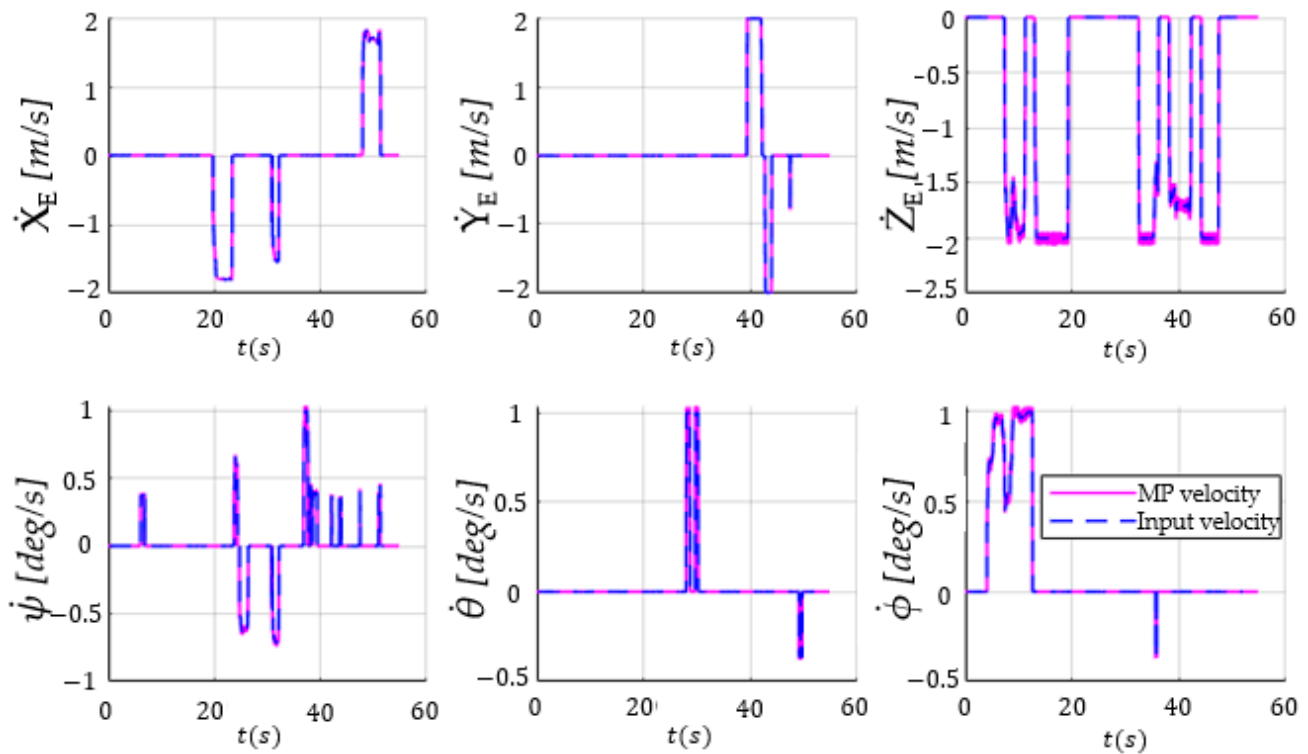


**Figure 22.** The time history diagram showing input velocity vectors (translations and rotations along and around the OX, OY, and OZ axes) using the 3D Space Mouse devices (the dashed blue lines) and the Mobile Platform (MP) velocities (the magenta lines).

#### 4. Discussion

This paper presents the control architecture and preliminary validation results performed under laboratory conditions. A master–slave architecture was implemented, where the master console consists of two commercially available devices (3D Space Mouse, version Space Mouse Pro, developed by 3DConnexion, Munich, Germany, 2001), with each offering six-DOF. This setup is well-suited for the six-DOF parallel robot that controls the laparoscope and positions the robotic modules responsible for manipulating the laparoscopic instruments. The master console generates linear and angular velocity vectors, which are further used to control the mobile platform. The developed GUI incorporates controls that facilitate switching seamless transitions between the parallel robot control and the manipulation modules for the surgical instruments attached to the mobile platform. Notably, the same master console is also used to manipulate the tips of the surgical instruments.

Based on the results presented in Figure 22, namely, the comparative time history diagram of the velocity vectors for both the input (generated by the master console) and output (resulting from the actuators' displacements), it can be concluded that the output closely tracked the input signal. It is important to note that there was a significant difference in the sampling time of the recordings (input vs. output signals), namely,  $\sim 0.01891$  s (with a standard deviation of 0.0065) vs. 0.005 s, respectively, which is why the output signal had approximately eight times more values than the input one (23,822 vs. 2747). To compute the root-mean-square error between the two signals, the input signal, which had fewer values, was interpolated using the “spline” method in matrix laboratory (MATLAB). The spline method has provided good results [52] for 1D vectors compared with linear or even polynomial interpolation. Even if it can be a source of errors when comparing the input–output signals, the accuracy of the spline interpolation is expected to be good because of the large number of points. The normalized results are presented in Table 2.

**Table 2.** Medical protocol used to perform the experimental tests with the PARA-SILSROB in the laboratory.

Velocity Vector Component	RMSE Value
$\dot{X}_E$	0.011591
$\dot{Y}_E$	0.017855
$\dot{Z}_E$	0.068058
$\dot{\psi}$	0.049791
$\dot{\theta}$	0.030903
$\dot{\varphi}$	0.022791

The RMSE values obtained for the PARA-SILSROB were very good, which was anticipated. These values validated the efficiency of the implemented control system, thus demonstrating its strong response to arbitrary input signals and the spline interpolation as well. Furthermore, they also validated the reliability of the robotic system itself. The potential sources of error outlined in Table 2 can be affected by factors such as system calibration, the sensors used during the calibration process, latency in the command and control system, vastly different sampling time between the input signal (the 3D Space Mouse), the output signal, the interpolation method, and the error of the Newton–Raphson numerical method used to compute the forward kinematic solution (where a fixed and relatively small number of iterations was used to decrease the computation time). To mitigate some of these errors, improvements were made to the control logic, the mechanical structure was recalibrated, and a threshold was implemented in the control logic to account for disturbances caused by erroneous readings from the two 3D Space Mouse devices. Compared with the results presented in [53–55], the errors obtained during the testing phase of the PARA-SILSROB robot (Table 2) validated both the functionality of the mechanical structure and the robustness of the command-and-control system.

The accurate positioning and orientation of the laparoscopic camera and instruments depend heavily on the mechanical architecture, including the gears, transmissions, and various machined parts of the robot. Each of these components were meticulously selected and crafted to ensure optimal performance. Furthermore, the repeatability and accuracy of the robot were tested using two measurement systems presented in detail in [56], demonstrating that the robot had good repeatability and accuracy for its first iteration. Additionally, while the robot was in operation, the user had the capability to visually confirm and adjust the pose of the robot and its modules within the surgical field, which allowed for real-time correction until the desired poses were achieved.

The two testing stages of the robot, which were conducted by medical experts, with one using a surgical kit and the other using a human phantom with 3D-printed esophagus, were used to evaluate the robotic system’s usability across various criteria: comfort, responsiveness, accuracy, injury risks for the patient, maintenance, and procedure timing. In terms of comfort, there was no significant negative feedback provided, where the surgeons were asked at the end of the tests to provide a value between 0 and 10 (where 0 represented a high level of discomfort and 10 represented a high level of comfort) for the comfort experienced during the use of the system. The majority assigned values between 8 and 10. However, it was suggested that a dedicated master console be developed that aligns more closely with the manual manipulation of instruments to facilitate a more intuitive interaction between the master and slave systems. Regarding the system responsiveness, it had a value of 5 milliseconds, which is below the human reaction time (200–300 milliseconds) and accuracy; no substantial issues were reported due to the visual nature of the control system. Nonetheless, the motion scalability (accessible via the GUI) was frequently used. The safety features of the robotic system also underwent rigorous testing. These features include automatic retraction of the surgical instruments, emergency stop procedures, motion-scaling capabilities, and software limits (designed to prevent singular configurations). The automatic retraction procedure for the instruments was implemented during the initial phase of

robot testing using the laparoscopic kit. This process involves displaying an error message on the graphical interface, which requires the surgeon to confirm by pressing a button (customizable to the surgeon's preferences) on either of the two 3D Space Mouse devices on the master console. Once the button is pressed and the surgeon confirms the initiation of the process, the instrument tips are moved to the home position. Upon reaching this position, the surgeon confirms it by pressing the same button again. After this confirmation, the instruments are automatically retracted from the intraoperative field.

For the emergency stop procedure, a dedicated button is provided on the engineer's graphical interface, which decelerates the robot's motors to zero, thus preventing a sudden halt. Additionally, motion scaling is limited by the software, with the system's maximum velocity and acceleration set at 25 mm/s and 50 mm/s<sup>2</sup>, respectively. These speed and acceleration settings can be adjusted according to the surgeon's preferences during the pre-planning stage.

A final safety measure restricts the motion range of each robot arm to prevent the system from reaching singularity positions or exceeding the end of the stroke. These constraints are encoded in the control system's source program, with additional safety measures that include displaying warnings on the surgeon's graphical interface when the robot approaches these critical positions.

One challenge identified during testing was the initial learning curve associated with setting up the robot. More specifically, aligning the RCM of the MP and the two modules that manipulate the surgical instruments with the trocars of the SILS port presented some difficulties. This procedure is performed manually, as the RCM registration requires visual confirmation, which requires a certain level of experience with the robot. However, following initial training, this procedure was completed much faster during the second stage of the validation tests.

In both testing stages, the surgeon encountered challenges in manipulating the robot due to the current limitations, such as the confined intraoperative space, the lack of tactile feedback, and the varying complexity of the operations performed during this testing phase. Despite these drawbacks, the tests were ultimately successful. However, the suturing operation proved particularly difficult and highlighted the need for further training with the robot. The necessity of a surgical simulator for PARA-SILSROB became obvious and should be prioritized before proceeding to the next stages of the robot's development.

It is worth mentioning that robotic surgery could improve esophageal surgery by ensuring the safe use of SILS with a faster learning curve. Robotic surgery seems like the natural step forward in the advancement of minimally invasive surgery, but it is not widely adopted yet, especially due to the higher prices compared with traditional laparoscopic surgery.

The platform has not been tested in simulated intraoperative conditions, which are the scope of further studies, including using live animal surgery, to better assess the operative benefits of PARA-SILSROB robotic system.

## 5. Conclusions

This study focused on the development of the control system of a robot designed for single-incision laparoscopic surgery. The system utilizes the master–slave architecture, where the master console consists of two commercially available 3D Space Mouse devices and a GUI. The slave consists of a six-DOF parallel robot, which guides the laparoscope and includes two modules for the manipulation of active surgical instruments. A state machine was integrated into the PLC that controls the robot's operations and incorporates specific control functions. The effectiveness of the control system was validated by comparing the desired input signals for the end effector with the actuators' response signal.

The robotic system was validated in laboratory conditions through a two-stage battery of tests. The first stage assessed the robot's functionality using a surgical kit to simulate a variety of operations and procedures used in robot-assisted surgery, including manipulation, resection, and suturing. The second stage simulated an esophagectomy and reconstruction

performed during the Ivor–Lewis procedure. For this simulation, a torso was used in which the main organs pertinent to this surgical procedure were accurately positioned. The organs used in this testing stage were modeled using image segmentation based on helical CT scans, and their simplified model was printed using the PolyJet 3D printing technique with soft materials.

Future research will focus on designing our custom active instruments, and additionally, efforts will concentrate on improving the current graphical interface, developing a surgical simulator to improve the learning curve, and finding ways to integrate tactile/haptic feedback into the active instruments by using two haptic devices and force sensors mounted on the flanges of the active instruments, along with enhanced visualization through a 3D HD laparoscope.-

**Author Contributions:** Conceptualization, D.P.; methodology, B.G., C.V. and D.C.; software, A.-D.C.; validation, A.C., C.P., E.M. and N.A.H.; formal analysis, B.G., D.C., A.P., A.C., C.R. and N.A.H.; investigation, A.P.; resources, D.P.; data curation, B.G. and C.V.; writing—original draft preparation, A.P., B.G. and A.-D.C.; writing—review and editing, D.P.; visualization, A.C.; supervision, D.P.; project administration, D.P. and D.C.; funding acquisition, D.P. and D.C. All authors have read and agreed to the published version of the manuscript.

**Funding:** This research was funded by the project New smart and adaptive robotics solutions for personalized minimally invasive surgery in cancer treatment—ATHENA, funded by the European Union—NextGenerationEU and Romanian Government, under National Recovery and Resilience Plan for Romania, contract no. 760072/23.05.2023, code CF 116/15.11.2022, through the Romanian Ministry of Research, Innovation and Digitalization, within Component 9, investment I8.

**Institutional Review Board Statement:** Not applicable.

**Informed Consent Statement:** Not applicable.

**Data Availability Statement:** The original contributions presented in the study are included in the article, further inquiries can be directed to the corresponding author.

**Conflicts of Interest:** The authors declare no conflicts of interest.

## References

1. Zhao, Z.; Jin, G. Open surgery in the era of minimally invasive surgery. *Chin. J. Cancer Res. Chung-Kuo Yen Cheng Yen Chiu* **2022**, *34*, 63–65. [[CrossRef](#)] [[PubMed](#)]
2. Patil, M., Jr.; Gharde, P.; Reddy, K.; Nayak, K. Comparative Analysis of Laparoscopic Versus Open Procedures in Specific General Surgical Interventions. *Cureus* **2024**, *16*, e54433. [[CrossRef](#)] [[PubMed](#)]
3. Pisla, D.; Crisan, N.; Gherman, B.; Andras, I.; Tucan, P.; Radu, C.; Pusca, A.; Vaida, C.; Al Hajjar, N. Safety Issues in the Development of an Innovative Medical Parallel Robot Used in Renal Single-Incision Laparoscopic Surgery. *J. Clin. Med.* **2023**, *12*, 4617. [[CrossRef](#)]
4. Othman, W.; Lai, Z.A.; Abril, C.; Barajas-Gamboa, J.S.; Corcelles, R.; Kroh, M.; Qasaimeh, M.A. Tactile Sensing for Minimally Invasive Surgery: Conventional Methods and Potential Emerging Tactile Technologies. *Front. Robot. AI* **2022**, *8*, 705662. [[CrossRef](#)] [[PubMed](#)]
5. Vladescu, C.; Copaescu, C. The Use of Minimal Invasive Surgery versus Open Approach in Hospitalized Cases. *Chirurgia (Bucur)* **2021**, *116*, 1–13. [[CrossRef](#)]
6. Harky, A.; Chaplin, G.; Chan, J.S.; Eriksen, P.; MacCarthy-Ofosu, B.; Theologou, T.; Muir, A.D. The Future of Open Heart Surgery in the Era of Robotic and Minimal Surgical Interventions. *Heart Lung Circ.* **2020**, *29*, 49–61. [[CrossRef](#)]
7. Darzi, S.A.; Munz, Y. The impact of minimally invasive surgical techniques. *Annu. Rev. Med.* **2004**, *55*, 223–237. [[CrossRef](#)]
8. Koo, Y.J. Recent advances in minimally invasive surgery for gynecologic indications. *Yeungnam Univ. J. Med.* **2018**, *35*, 150–155. [[CrossRef](#)]
9. Mangone, P.; Bitterman, A.; Brigido, S.A.; Cooper, M.T. Both the Benefits and Disadvantages of Minimally Invasive Surgery. *Foot Ankle Spec.* **2019**, *12*, 546–548. [[CrossRef](#)]
10. Zhao, L.; Kong, X.; Li, J.; Huang, L.; Xia, C.; Xu, J. Transumbilical single-incision laparoscopic pancreatoduodenectomy. *Asian J. Surg.* **2022**, *45*, 888–889. [[CrossRef](#)]
11. Greaves, N.; Nicholson, J. Single incision laparoscopic surgery in general surgery: A review. *Ann. R. Coll. Surg. Engl.* **2011**, *93*, 437–440. [[CrossRef](#)]



12. Vaida, C.; Andras, I.; Birlescu, I.; Crisan, N.; Plitea, N.; Pisla, D. Preliminary control design of a Single-Incision Laparoscopic Surgery Robotic System. In Proceedings of the 2021 25th International Conference on System Theory, Control and Computing (ICSTCC), Iasi, Romania, 20–23 October 2021; pp. 384–389. [CrossRef]
13. Schneider, B.; Brockhaus, A.C.; Gelos, M.; Rudroff, C. The single-incision laparoscopic surgery technique has questionable advantages in colorectal surgery. *Innov. Surg. Sci.* **2018**, *3*, 77–84. [CrossRef]
14. Saidy, M.N.; Tessier, M.; Tessier, D. Single-incision laparoscopic surgery—hype or reality: A historical control study. *Perm J.* **2012**, *16*, 47–50. [CrossRef] [PubMed]
15. drheidarizadi.com. Available online: <https://drheidarizadi.com/learning-center/single-port-surgery.html> (accessed on 3 July 2024).
16. Morrell, A.L.G.; Morrell-Junior, A.C.; Morrell, A.G.; Mendes, J.M.F.; Tustumi, F.; DE-Oliveira-E-Silva, L.G.; Morrell, A. The history of robotic surgery and its evolution: When illusion becomes reality. *Rev. Colégio Bras. Cir.* **2021**, *48*, e20202798. [CrossRef] [PubMed]
17. George, E.I.; Brand, T.C.; LaPorta, A.; Marescaux, J.; Satava, R.M. Origins of Robotic Surgery: From Skepticism to Standard of Care. *JSLS J. Soc. Laparosc. Robot. Surg.* **2018**, *22*, e2018-00039. [CrossRef] [PubMed]
18. Thai, M.T.; Phan, P.T.; Hoang, T.T.; Wong, S.; Lovell, N.H.; Do, T.N. Advanced Intelligent Systems for Surgical Robotics. *Adv. Intell. Syst.* **2022**, *2*, 1900138. [CrossRef]
19. Low, S.C.; Phee, L. A review of master-slave robotic systems for surgery. In Proceedings of the IEEE Conference on Robotics, Automation and Mechatronics 2004, Singapore, 1–3 December 2004; Volume 1, pp. 37–42. [CrossRef]
20. Pisla, D.; Gherman, B.; Tucan, P.; Birlescu, I.; Pusca, A.; Rus, G.; Pisla, A.; Vaida, C. Application Oriented Modelling and Simulation of an Innovative Parallel Robot for Single Incision Laparoscopic Surgery. In Proceedings of the ASME 2022 International Design Engineering Technical Conferences and Computers and Information in Engineering Conference. Volume 7: 46th Mechanisms and Robotics Conference (MR), St. Louis, MO, USA, 14–17 August 2022. [CrossRef]
21. Ballantyne, G.H. Robotic surgery, telerobotic surgery, telepresence, and telementoring. Review of early clinical results. *Surg Endosc.* **2002**, *16*, 1389–1402. [CrossRef]
22. Silverman, C.; Isaacs, A.; Tan, N.G. Robotic bariatric surgery. In *Obesity and Diabetes: Scientific Advances and Best Practice*; Springer: Berlin/Heidelberg, Germany, 2020; pp. 791–812. [CrossRef]
23. radroboticsurgery.com. Available online: <https://www.radroboticsurgery.com/post/roboticsurgery> (accessed on 4 July 2024).
24. Bhat, K.R.S.; Moschovas, M.C.; Onol, F.F.; Rogers, T.; Reddy, S.S.; Corder, C.; Roof, S.; Patel, V.R. Evidence-based evolution of our robot-assisted laparoscopic prostatectomy (RALP) technique through 13,000 cases. *J. Robot. Surg.* **2021**, *15*, 651–660. [CrossRef]
25. Intuitive.com. Available online: <https://www.intuitive.com/en-us/products-and-services/da-vinci> (accessed on 4 July 2024).
26. McCarus, S.D. Senhance Robotic Platform System for Gynecological Surgery. *JSLS J. Soc. Laparosc. Robot. Surg.* **2021**, *25*, e2020-00075. [CrossRef]
27. Dobbs, R.W.; Halgrimson, W.R.; Talamini, S.; Vigneswaran, H.T.; Wilson, J.O.; Crivellaro, S. Single-port robotic surgery: The next generation of minimally invasive urology. *World J. Urol.* **2020**, *38*, 897–905. [CrossRef]
28. Vaida, C.; Pisla, D.; Schadlbauer, J.; Husty, M.; Plitea, N. Kinematic analysis of an innovative medical parallel robot using study parameters. In *New Trends in Medical and Service Robots. Mechanisms and Machine Science*; Wenger, P., Chevallereau, C., Pisla, D., Bleuler, H., Rodić, A., Eds.; Springer: Cham, Switzerland, 2016; Volume 39. [CrossRef]
29. Rivero-Moreno, Y.; Echevarria, S.; Vidal-Valderrama, C.; Pianetti, L.; Cordova-Guilarte, J.; Navarro-Gonzalez, J.; Acevedo-Rodríguez, J.; Dorado-Avila, G.; Osorio-Romero, L.; Chavez-Campos, C.; et al. Robotic Surgery: A Comprehensive Review of the Literature and Current Trends. *Cureus* **2023**, *15*, e42370. [CrossRef]
30. Pisla, D.; Birlescu, I.; Vaida, C.; Tucan, P.; Pisla, A.; Gherman, B.; Crisan, N.; Plitea, N. Algebraic modeling of kinematics and singularities for a prostate biopsy parallel robot. *Proc. Rom. Acad. Ser. A* **2018**, *19*, 489–497.
31. generalsurgerynews.com. Available online: <https://www.generalsurgerynews.com/In-the-News/Article/07-22/Robotic-Surgery/67443?ses=ogst> (accessed on 4 July 2024).
32. Antonilli, M.; Sevas, V.; Luisa Gasparri, M.; Ahmad Farooqi, A.; Papadia, A. Minimally Invasive Surgery in Gynecology. *Adv. Minim. Invasive Surg.* **2021**, 1–16. [CrossRef]
33. Muaddi, H.; Hafid, M.E.; Choi, W.J.; Lillie, E.; de Mestral, C.; Nathens, A.; Stukel, T.A.; Karanicolas, P.J. Clinical Outcomes of Robotic Surgery Compared to Conventional Surgical Approaches (Laparoscopic or Open): A Systematic Overview of Reviews. *Ann. Surg.* **2021**, *273*, 467–473. [CrossRef]
34. Gómez Ruiz, M.; Lainez Escribano, M.; Cagigas Fernández, C.; Cristobal Poch, L.; Santarrufina Martínez, S. Robotic surgery for colorectal cancer. *Ann. Gastroenterol. Surg.* **2020**, *4*, 646–651. [CrossRef] [PubMed]
35. Liu, B.; Li, X.; Yu, M.J.; Xie, J.B.; Liao, G.L.; Qiu, M.L. Application of single-port laparoscopic retrograde gastric mobilization during McKeown esophagectomy for esophageal cancer. *Ann. Thorac. Med.* **2023**, *18*, 39–44. [CrossRef]
36. Huang, Y.H.; Chen, K.C.; Lin, S.H.; Huang, P.M.; Yang, P.W.; Lee, J.M. Robotic-assisted single-incision gastric mobilization for minimally invasive oesophagectomy for oesophageal cancer: Preliminary results. *Eur. J. Cardiothorac. Surg.* **2020**, *58* (Suppl. 1), i65–i69. [CrossRef] [PubMed]
37. Leng, X.; Seto, Y. Robot-assisted transmediastinal esophagectomy: The path of concept and practice. *Intell. Surg.* **2023**, *6*, 61–63. [CrossRef]

38. Tucan, P.; Birlescu, I.; Pusca, A.V.; Gherman, B.; Jucan, D.; Antal, T.; Vaida, C.; Pisla, A.; Chablat, D.; Pisla, D. A Flexible Instrument for Robotic Assisted Minimally Invasive Esophagectomy. In *New Trends in Mechanism and Machine Science*; EuCoMeS 2024. Mechanisms and Machine Science; Rosati, G., Gasparetto, A., Ceccarelli, M., Eds.; Springer: Cham, Switzerland, 2024; Volume 165. [CrossRef]
39. Xu, Q.L.; Li, H.; Zhu, Y.J.; Xu, G. The treatments and postoperative complications of esophageal cancer: A review. *J. Cardiothorac. Surg.* **2020**, *15*, 163. [CrossRef]
40. Narayan, J.; Singla, E.; Soni, S.; Singla, A. Adaptive neuro-fuzzy inference system-based path planning of 5-degrees-of-freedom spatial manipulator for medical applications. *Proceedings of the Institution of Mechanical Engineers. Part H J. Eng. Med.* **2018**, *232*, 726–732. [CrossRef]
41. Singla, A.; Narayan, J.; Arora, H. Investigating the potential of redundant manipulators in narrow channels. *Proc. Inst. Mech. Eng. Part C J. Mech. Eng. Sci.* **2021**, *235*, 3723–3736. [CrossRef]
42. Barron, J.O.; Blackstone, E.H.; Rice, T.W.; Lowry, A.M.; Tasnim, S.; Toth, A.J.; Murthy, S.C.; Raja, S. Cleveland Clinic Thoracic Surgery Research Group and Worldwide Esophageal Cancer Collaboration Investigators. Thoracoabdominal Esophagectomy: Then and Now. *Ann. Thorac. Surg.* **2024**, *118*, 402–411. [CrossRef] [PubMed]
43. Pisla, D.; Pusca, A.; Tucan, P.; Gherman, B.; Vaida, C. Kinematics and workspace analysis of an innovative 6-dof parallel robot for SILS. *Proc. Rom. Acad. Ser. A* **2022**, *23*, 279–288.
44. Zhou, X.; Zhang, H.; Feng, M.; Zhao, J.; Fu, Y. New remote centre of motion mechanism for robot-assisted minimally invasive surgery. *Biomed. Eng. Online* **2018**, *17*, 170. [CrossRef]
45. Siemens PLM Software. Available online: <https://plm.sw.siemens.com/en-US/nx/cad-online/> (accessed on 19 June 2024).
46. Pusca, A.; Andras, I.; Cailean, A.; Crisan, N.; Vaida, C.; Radu, C.; Pisla, D. On the Development of an Innovative Surgical Parallel Robotic System. In *Advances in Digital Health and Medical Bioengineering*; EHB 2023. IFMBE Proceedings; Costin, H.N., Magjarević, R., Petroiu, G.G., Eds.; Springer: Cham, Switzerland, 2023; Volume 109, pp. 173–183. [CrossRef]
47. Pisla, D.; Calin, V.; Birlescu, I.; Hajjar, N.A.; Gherman, B.; Radu, C.; Plitea, N. Risk Management for the Reliability of Robotic Assisted Treatment of Non-resectable Liver Tumors. *Appl. Sci.* **2020**, *10*, 52. [CrossRef]
48. Pisla, D.; Nadas, I.; Tucan, P.; Albert, S.; Carbone, G.; Antal, T.; Banica, A.; Gherman, B. Development of a Control System and Functional Validation of a Parallel Robot for Lower Limb Rehabilitation. *Actuators* **2021**, *10*, 277. [CrossRef]
49. Vaida, C.; Rus, G.; Gherman, B.; Pusca, A.; Tucan, P.; Ulinici, I.; Pisla, D. Development of an augmented reality simulator for a robotic system used in single incision laparoscopic surgery. *The Romanian Journal of Technical Sciences. Appl. Mech.* **2023**, *68*, 3–18. [CrossRef]
50. Vaida, C.; Gherman, B.; Birlescu, I.; Tucan, P.; Pusca, A.; Rus, G.; Chablat, D.; Pisla, D. Kinematic Analysis of a Parallel Robot for Minimally Invasive Surgery. In *Advances in Robot Kinematics 2024*; ARK 2024. Springer Proceedings in Advanced Robotics; Lenarčič, J., Husty, M., Eds.; Springer: Cham, Switzerland, 2024; Volume 31. [CrossRef]
51. Valls-Esteve, A.; Adell-Gómez, N.; Pasten, A.; Barber, I.; Munuera, J.; Krauel, L. Exploring the Potential of Three-Dimensional Imaging, Printing, and Modeling in Pediatric Surgical Oncology: A New Era of Precision Surgery. *Children* **2023**, *10*, 832. [CrossRef]
52. Yang, B.; Li, Y.; Zheng, W.; Yin, Z.; Liu, M.; Yin, L.; Liu, C. Motion prediction for beating heart surgery with GRU. *Biomed. Signal Process. Control* **2023**, *83*, 104641. [CrossRef]
53. Hamedani, M.H.; Selvaggio, M.; Rahimkhani, M.; Ficuciello, F.; Sadeghian, H.; Zekri, M.; Sheikholeslam, F. Robust Dynamic Surface Control of da Vinci Robot Manipulator Considering Uncertainties: A Fuzzy Based Approach. In *Proceedings of the 2019 7th International Conference on Robotics and Mechatronics (ICRoM)*, Tehran, Iran, 20–21 November 2019; pp. 418–423. [CrossRef]
54. Roberti, A.; Piccinelli, N.; Meli, D.; Muradore, R.; Fiorini, P. Improving Rigid 3-D Calibration for Robotic Surgery. *IEEE Trans. Med. Robot. Bionics* **2020**, *2*, 569–573. [CrossRef]
55. Shi, H.; Liu, Q.; Mei, X. Accurate Parameter Estimation for Master–Slave Operation of a Surgical Robot. *Machines* **2021**, *9*, 213. [CrossRef]
56. Pisla, D.; Tucan, P.; Chablat, D.; Al Hajjar, N.; Ciocan, A.; Pusca, A.; Pisla, A.; Radu, C.; Pop, G.; Gherman, B. Accuracy and Repeatability of a Parallel Robot for Personalised Minimally Invasive Surgery. In *Advances in Service and Industrial Robotics*; RAAD 2024. Mechanisms and Machine Science; Pisla, D., Carbone, G., Condurache, D., Vaida, C., Eds.; Springer: Cham, Switzerland, 2024; Volume 157, pp. 185–195. [CrossRef]

**Disclaimer/Publisher’s Note:** The statements, opinions and data contained in all publications are solely those of the individual author(s) and contributor(s) and not of MDPI and/or the editor(s). MDPI and/or the editor(s) disclaim responsibility for any injury to people or property resulting from any ideas, methods, instructions or products referred to in the content.